RESEARCH ARTICLE

# Subunit-specific roles of LRRC8 proteins in determining glutamate permeability of astrocytic volume-regulated anion channels

**Madison L. Chandler, Ariella D. Sprague, Julia W. Nalwalk, and Alexander A. Mongin***

*Department of Neuroscience and Experimental Therapeutics, Albany Medical College, Albany, New York, United States*

*Correspondence: Dr. Alexander A. Mongin, Department of Neuroscience and Experimental Therapeutics, Albany Medical College, 47 New Scotland Avenue, Albany, NY 12208, United States. Email: mongina@amc.edu; phone: +1-518-262-9052.

Running Head: COMPOSITION OF ASTROCYTIC LRRC8/VRAC CHANNELS

## ABSTRACT

Volume-regulated anion channels (VRACs) are ubiquitous chloride channels that play important roles in cell volume regulation and numerous other physiological processes. VRACs are heteromeric complexes composed of leucine-rich repeat-containing proteins LRRC8A-E. LRRC8 subunit composition determines biophysical properties of VRACs, including permeability to small signaling molecules. Here, we used primary astrocyte cultures from wild-type and genetically modified C57BL/6 mice to investigate (i) subunit composition of native VRACs in the brain and (ii) subunit determinants of VRAC permeability to the excitatory neurotransmitter glutamate. qRT-PCR and RNA-seq analyses revealed high expression of *Lrrc8a-d* in mouse forebrain and astrocytes. Genetic deletion of the essential LRRC8A protein abolished swelling-activated glutamate release, measured as efflux of the non-metabolizable D-[$^3$H]aspartate, confirming the crucial role of VRACs in this process. RNAi-mediated knockdown of individual subunits identified LRRC8A and LRRC8C as key components of glutamate-permeable astrocytic VRACs. qRT-PCR and Western blot analyses further showed that knockdown of LRRC8A or LRRC8C reciprocally altered the protein stability of the partner subunit without affecting their mRNA levels. A similar pattern of mutual regulation was observed between LRRC8A and LRRC8D. In contrast to LRRC8C, downregulation of LRRC8D had a more limited impact on glutamate release. Additional double-knockdown experiments demonstrated that LRRC8C- and LRRC8D-containing channels form distinct VRAC populations. This model was further supported by Western blot results showing no reciprocal regulation of LRRC8C and LRRC8D stability. Together, these findings refine our understanding of how the subunit organization of native brain VRACs governs gliotransmitter release, with implications for normal brain function and neurological disease.


## NEW & NOTEWORTHY

Volume-regulated anion channels (VRACs) are ubiquitously expressed chloride channels composed of LRRC8A-E proteins. In human disorders, gain or loss of VRAC function leads to severe neurological phenotypes, potentially due to altered release of amino acid neurotrans-mitters. Here, we show that glutamate-permeable VRACs in brain astrocytes are primarily composed of LRRC8A and LRRC8C proteins. These findings provide insight into subunit organization of native VRACs in the CNS, with implications for normal brain function and neurological disease.


**Keywords:** Astrocytes, Glutamate release, LRRC8, LRRC8A, VRAC

# INTRODUCTION

Volume-regulated anion channels (VRACs), also known as volume-sensitive outwardly rectifying anion channels (VSOR) or volume-sensitive organic osmolyte/anion channels (VSOAC), are swelling-activated chloride ($Cl^-$) channels found in virtually all vertebrate cells (1-3). VRAC activity is typically assessed by measuring swelling-induced $Cl^-$ currents ($I_{Cl,vol}$) in cells exposed to hypoosmotic media [e.g., early studies (4-7)]. However, in addition to $Cl^-$, VRACs are also permeable to a range of small negatively charged or uncharged organic molecules, collectively referred to as organic osmolytes (1, 8-11). As their name implies, VRACs play a key role in cell volume control and mediate regulatory volume decrease (RVD), a fundamental physiological process that restores cell volume after osmotic swelling. RVD is driven primarily by the electrically coupled efflux of cytosolic $Cl^-$ (via VRACs) and $K^+$ (via separate $K^+$ channels), with additional contributions from bicarbonate and organic osmolytes (12, 13). Beyond their role in RVD, VRACs have been implicated in numerous other physiological and pathological processes, including regulation of membrane potential, cell proliferation, apoptosis, immune responses, and paracrine signaling [reviewed in (14-19)].

Historically, investigation of cell- and tissue-specific VRAC functions was hindered by the unknown molecular identity of these channels (20-22). A major breakthrough occurred in 2014 when the laboratories of Ardem Patapoutian and Thomas Jentsch independently used genome-wide siRNA screens to identify leucine-rich repeat-containing family 8 member A (LRRC8A, also known as SWELL1) as an essential component of VRACs (23, 24). LRRC8A belongs to a family of five LRRC8 proteins (LRRC8A-E) that share an evolutionary origin with vertebrate pannexins (25). Whole-body deletion of LRRC8A is embryonically and postnatally lethal, with ~80% of LRRC8A-null mice dying in utero and the remaining live-born animals succumbing rapidly to multi-organ failure (26). In contrast, tissue- and cell type-specific deletions of LRRC8A are generally better tolerated [e.g., (27-29)]. Consistent with this pattern, mice with brain-specific LRRC8A knockout (bLRRC8A KO, generated by $Nestin^{Cre}$-driven recombination) are born at expected Mendelian ratios and display no overt abnormalities in brain development (30). However, bLRRC8A KO animals unexpectedly develop spontaneous seizures and all die during late adolescence or early adulthood (30, 31), highlighting the critical yet poorly understood role of VRACs in the regulation of neural excitability.

Although VRACs can modulate neuronal activity via multiple mechanisms, their influence over brain excitability is usually attributed to their permeability to amino acid-derived neuro-transmitters and modulators (15, 32-34). VRACs conduct excitatory glutamate and aspartate, as well as inhibitory GABA and taurine (8, 9, 11). Within the brain, astrocytes are thought to be the main site of physiological and pathological VRAC activity due to the propensity of these cells to swell in response to neuronal excitation or brain injury (34-36). Under physiological conditions, limited opening of astrocytic VRACs is also seen in response to GPCR-driven increases in intracellular $Ca^{2+}$ (28, 37-39). In vivo, conditional deletion of astrocytic LRRC8A reduces tonic glutamate and GABA signaling and modifies animal behavior (28, 40). VRACs' influence becomes even more pronounced in neural pathologies that promote pathological cell swelling, such as stroke, traumatic brain injury, and epilepsy (15, 34-36). In animal stroke models, putative but structurally diverse VRAC blockers—tamoxifen, DCPIB, dicoumarol, and bromadiolone—strongly reduce ischemic brain injury (41-45), and this effect is partially recapitulated in bLRRC8A KO mice (28, 31, 46), highlighting VRAC as an attractive therapeutic target.

Given the emerging importance of VRACs in brain health and disease, there is strong interest in their molecular structure and function. Cryo-electron microscopy studies have established that LRRC8 proteins assemble into hexameric channels with one central ion-conducting pore (47-52). The essential LRRC8A protein must co-assemble with at least one additional isoform—LRRC8C, LRRC8D, or LRRC8E—to form fully functional VRACs (24). The partnering LRRC8B-E subunits are expressed in a cell- and tissue-specific manner and confer functional diversity to VRACs, including differential permeability to organic osmolytes (16, 18, 19, 21). For example, LRRC8A/LRRC8D heteromers preferentially conduct small uncharged molecules and zwitterions, including myo-inositol, taurine, GABA, and glutamine (53-55). In contrast, there is little consensus on the subunit organization of VRACs permeable to negatively charged glutamate and aspartate, with several studies reporting different LRRC8 assemblies depending on cell type [see refs. (54-56) and Discussion]. This represents an important gap in knowledge since VRAC-driven glutamate release is thought to play an important role in both the physiological and pathological regulation of brain excitability. Hence, in the present study, we sought to identify the LRRC8 subunits that confer glutamate permeability to endogenous VRACs in primary mouse astrocytes.

# MATERIALS AND METHODS

## Ethical Approval

All animal procedures used in the present study were approved by the Institutional Animal Care and Use Committee of Albany Medical College (ACUP 24-03002), and strictly conformed to the Guide for the Care and Use of Laboratory Animals as adopted by the U.S. National Institutes of Health (https://grants.nih.gov/grants/olaw/guide-for-the-care-and-use-of-laboratory-animals.pdf).

## Animals

This study utilized two types of mice to collect brain tissue and generate primary astrocyte cultures. Wild type (WT) animals were of the C57BL/6J background, originally obtained from the Jackson Laboratory (Farmington, CT, USA; strain #000664, RRID: IMSR_JAX:000664) and bred in-house. Additionally, we used mice with conditional knockout of LRRC8A in the brain (bLRRC8A KO). These were produced by breeding *Lrrc8a*$^{flox/flox}$ females (gift of Dr. Rajan Sah, Washington University School of Medicine, St. Louis, MO, USA) with commercially available *Nestin*$^{Cre/+}$ males (B6.Cg-Tg(Nes-cre)1Kln/J; Jackson Lab stock #003771, RRID:IMSR_JAX:003771). Heterozygous *Nestin*$^{Cre/+}$:*Lrrc8a*$^{flox/+}$ males were further crossed with *Lrrc8a*$^{flox/flox}$ female mice to produce *Nestin*$^{Cre/+}$:*Lrrc8a*$^{flox/flox}$ mice (bLRRC8A KO) and littermate controls. The specificity and efficacy of this genetic strategy were thoroughly validated in our previous work (30, 46). To visualize Cre activity and monitor for unintentional germline recombination, mice were additionally inbred with a strain carrying the Ai9 tdTomato Cre reporter (B6.Cg-Gt(ROSA)26Sor$^{tm9(CAG\text{-}tdTomato)Hze}$/J; Jackson Lab stock #007909, RRID:IMSR_JAX:007909). For simplicity, the presence of the reporter allele is not shown in the breeding diagram. All mice were housed in a temperature, humidity, and light-controlled facility on a 12:12 h light/dark cycle and given free access to food and water.

143 ## Brain Tissue Collection and Processing

144 For brain tissue collection, 14-week-old WT mice were euthanized with a lethal injection
145 of sodium pentobarbital and perfused transcardially, first with room temperature phosphate-
146 buffered saline (PBS), followed by ice-cold PBS. For qRT-PCR analysis, brains were rapidly
147 removed and immediately transferred to a large dissection dish containing ice cold PBS
148 additionally treated with the RNase inhibitor diethyl pyrocarbonate (DEPC, 0.1%). The olfactory
149 bulbs, cerebellum and brainstem were removed, and a midline sagittal cut was made to separate
150 the hemispheres. Each hemisphere was snap-frozen in liquid nitrogen and stored at –80$^{o}$C until
151 further processing.

152

153 ## Primary Cultures of Mouse Astrocytes

154 Primary cultures of mouse astrocytes were prepared from brain cortices of newborn (P0-
155 P2) pups of both sexes as most recently described in (46) with minor modifications. Briefly,
156 neonates were anesthetized by cooling and rapidly decapitated. Brains were harvested and
157 transferred into ice-cold sterile Dulbecco's PBS without calcium and magnesium (ThermoFisher
158 Scientific, Waltham, MA, USA, cat. #14190144). Cortical tissue was dissected from meninges,
159 minced using a sterile surgical blade, incubated with 500 µL of the recombinant protease TrypLE
160 Express (ThermoFisher, cat. #12605) and additionally triturated by pipetting. Triturated tissue was
161 digested with TrypLE for 5 min at room temperature (22$^{o}$C). Enzymatic digestion was terminated
162 by adding Earl's minimal essential medium (MEM, ThermoFisher, cat. #11095) supplemented
163 with 10% heat-inactivated horse serum (HIHS, ThermoFisher, cat. #26050) and
164 penicillin/streptomycin (P/S, ThermoFisher, cat. #15140). The cell suspension was next filtered
165 through a 70-µm nylon mesh cell strainer (Corning, Corning, NY, USA, cat. # 431751). To obtain
166 an enriched astrocyte population, cells extracted from either half brain (for WT), or full brain
167 (bLRRC8A KO) were separately plated onto T75 flasks and grown in a humidified atmosphere of
168 5% $CO_2$/balance air at 37$^{o}$C. With this approach, primary cell cultures typically reached confluency
169 after around two weeks and were maintained for up to six weeks until replating for functional
170 assays. The purity of astrocyte populations was periodically verified with immunofluorescence by
171 staining for the astrocyte marker, glial fibrillary acidic protein (anti-GFAP, MilliporeSigma, St.
172 Louis, MO, USA, cat. #MAB360, RRID:AB_11212597; 1:400 dilution) and was ≥95%.

173

174 ## Quantitative Real-Time PCR (qRT-PCR)

175 Relative gene expression and efficacy of siRNA gene knockdowns were assessed using
176 qRT-PCR. Total RNA was isolated from brain tissue or primary astrocyte cultures using the Aurum
177 Total RNA Mini Kit (Bio-Rad, Hercules, CA, USA, cat. #732-6820) following the manufacturer's
178 instructions. Processing of tissue samples included on-column DNase digestion to eliminate
179 genomic DNA contamination. RNA concentration was measured with a NanoDrop 1000
180 spectrophotometer (ThermoFisher, RRID:SCR_016517). RNA was immediately converted to
181 cDNA using the iScript cDNA synthesis kit (Bio-Rad, cat. #1708891), with 1 µg of total RNA per
182 20 µL reaction. The resulting cDNA was analyzed for the relative abundance of *Lrrc8* transcripts
183 by qRT-PCR using gene-specific primers and SYBR Green Supermix (Bio-Rad, cat. #1708882)
184 in a CFX96 Real-Time PCR Detection System (Bio-Rad, RRID:SCR_018064). Expression levels
185 were normalized to the housekeeping gene *Rpl13a*, and where applicable, further normalized to

control samples using the $2^{-\Delta\Delta C(T)}$ method (57). As an internal quality control, expression of an additional housekeeping gene, *Rps20*, and the abundant transcript *Gapdh* were also quantified. All qRT-PCR primers were obtained as validated GeneGlobe assays from Qiagen (Germantown, MD, USA); detailed catalog information is provided in Table 1.

## Western Blotting

Protein levels of LRRC8A, LRRC8C, and LRRC8D were measured in lysates from primary astrocyte cultures. Cells were lysed in a denaturing buffer containing 2% sodium dodecyl sulfate (SDS) and 8 mM EDTA. Protein concentration was determined using the Pierce Bicinchoninic acid protein assay kit (Thermo Fisher Scientific, cat. #23225). The remaining lysate was diluted with 4× Laemmli sample buffer (Bio-Rad, cat. #4561033) and stored at −80°C until analysis. Lysates were boiled for 5 min, and 10-20 µg of total protein per sample was resolved on 10% Mini-PROTEAN TGX gels (Bio-Rad, cat. #1610747) via SDS-PAGE. Proteins were then transferred to polyvinylidene difluoride (PVDF) membranes (Bio-Rad, cat. #1620177) using a Trans-Blot Turbo transfer system (Bio-Rad, RRID:SCR_023156). Membranes were blocked for 20 min in Tris-buffered saline with 0.1% Tween-20 (TBS-T) containing 5% non-fat dry milk and further incubated with primary antibody overnight at 4°C. After washing in TBS-T, membranes were incubated for 2 h at room temperature with a species-matching HRP-conjugated secondary antibody in 5% milk/TBS-T. Protein bands were visualized using enhanced chemiluminescence reagent (ECL; GE Healthcare, cat. #RPN2232) and a ChemiDoc Imaging System (Bio-Rad, RRID:SCR_019684). For loading controls, membranes were washed and re-probed for 30 min with HRP-conjugated anti-β-actin antibody. Band intensities were quantified using ImageJ software (58) (NIH, RRID:SCR_003070) and were normalized to β-actin immunoluminescence from the same blot. Detailed information on all antibodies and their dilutions is provided in Table 2. For each antibody, we provide representative full-length Western blot images in the main figures. The complete dataset of analyzed Western blots, including matching β-actin loading controls, is included with Supplemental materials.

## RNAi-Mediated LRRC8 Gene Silencing

Targeted knockdown of LRRC8 family members was achieved using gene-specific siRNA constructs obtained from Qiagen (Valencia, CA, USA). AllStars Negative Control siRNA (Qiagen) was used as a non-targeting control. Primary astrocytes at ~70-80% confluency were transfected using Lipofectamine RNAiMAX (Thermo Fisher, cat. #13778075) according to the manufacturer's protocol. siRNA-Lipofectamine complexes were prepared in Opti-MEM (Thermo Fisher, cat. #31985), diluted further with Opti-MEM, and added to cells at final siRNA concentrations ranging from 10 to 50 nM (optimized for individual siRNAs). Details of the siRNA constructs, including catalog numbers and target sequences, are listed in Table 3. Knockdown efficacy for each construct was validated by qRT-PCR. After a 4h incubation, cultures were supplemented with MEM containing 10% HIHS and penicillin plus streptomycin (MEM+HIHS+P/S). At 24 h post-transfection, the medium was fully replaced with fresh MEM+HIHS+P/S. mRNA expression levels were assessed 48h post-transfection, and functional assays were performed 96h post-transfection.

## Radiotracer Assays of VRAC Activity

VRAC activity was evaluated by measuring the release of D-[$^3$H]aspartate, a non-metabolizable analog of glutamate, as extensively validated in our earlier studies [e.g., (55, 59, 60)]. Two complementary assay formats were used, employing astrocytes cultured either in multi-well plates or on glass coverslips. In all experiments, astrocytes were preloaded overnight in standard serum-containing medium supplemented with 2 µCi/mL D-[$^3$H]aspartate (Revvity, cat. #NET50100).

For medium-throughput screening of multiple siRNA constructs, cells were grown on poly-D-lysine-coated 12-well plates. After radiotracer loading, cultures were washed to remove extracellular isotope and equilibrated for 30 min at 37°C in isoosmotic Basal medium containing (in mM): 135 NaCl, 3.8 KCl, 1.2 $MgSO_4$, 1.3 $CaCl_2$, 1.2 $KH_2PO_4$, 10 D-glucose, and 10 HEPES (pH 7.4; osmolality 290 ±3 mOsm/kg). To inhibit radiotracer reuptake via $Na^+$-dependent GLAST transporters, cells were exposed to LiCl-substituted media, in which NaCl was isoosmotically replaced with LiCl (61). Baseline release was measured during a 10 min incubation in isoosmotic $Li^+$-containing medium, followed by stimulation with hypoosmotic $Li^+$ medium (LiCl reduced by 50 mM; final osmolality ~200 mOsm/kg, ~30% reduction) to activate VRACs. Ten-min fractions of isoosmotic and hypoosmotic media were collected for analysis. Radiotracer release was quantified by liquid scintillation counting using a TRI-CARB 4910TR counter (Revvity), after mixing samples with Ecoscint A scintillation fluid (National Diagnostics, cat. #LS-273). Integral release values were normalized to the remaining intracellular D-[$^3$H]aspartate, determined after cell lysis in 2% SDS containing 8 mM EDTA.

To resolve the kinetics of VRAC activation, D-[$^3$H]aspartate efflux assays were conducted using a custom-fabricated Lucite superfusion chamber that has a depression on the bottom to accommodate an 18 × 18 mm glass coverslip and a Teflon screw lid that leaves a ~200 µm space above the cells. Coverslips with D-[$^3$H]aspartate-preloaded astrocytes were briefly washed with Basal medium (for composition see above), transferred into the chamber, and superfused at a constant rate of ~1.4 mL/min with either isoosmotic or hypoosmotic media. In this setup, we used NaCl-containing media because released D-[$^3$H]aspartate was effectively removed with the flow. One-min perfusate fractions were collected into scintillation vials using an automated CF-1 fraction collector (SpectraLab Scientific, Markham, ON, Canada). At the conclusion of each experiment, cells were lysed in 2% SDS+8 mM EDTA, and D-[$^3$H]aspartate content in all samples was quantified using a scintillation counter as described above. Data were expressed as fractional release values, calculated at each time point as a ratio of released [$^3$H] to the total [$^3$H] content (cumulative release + remaining tracer), using a custom Excel-based analysis program.

## Statistics

All data are presented as mean values ± SD. The n value corresponds to an individual animal (qRT-PCR and RNA-seq) or an independently transfected astrocyte culture. For cell culture experiments, all results were reproduced in multiple cultures prepared from at least two different animals, unless specified otherwise. Statistical differences between three or more groups were analyzed using one-way ANOVA followed by Tukey's multiple comparisons test. In high-throughput functional assays, we used repeated-measures two-way ANOVA to assess the effects of medium (cell swelling), treatment (siRNA), and their interaction, followed by Tukey's multiple comparisons test. In several instances, to increase the clarity of the graphical presentation, we show only the most germane statistical effects; full analyses are included in the primary datasets deposited in the Open Science Framework (https://osf.io/xvyba). In RNAi expression assays, mRNA expression values were normalized to the expression levels in siNC-treated cells and

compared to unity using a one-sample t-test with Bonferroni correction for multiple comparisons. All statistical analyses and graphical preparations were performed using GraphPad Prism 10.0 (GraphPad Software, San Diego, CA, USA; RRID:SCR_002798).

# RESULTS

## LRRC8A Deletion Abolishes Activity of Glutamate-Permeable VRACs in Astrocytes

To investigate the role of LRRC8 proteins in the formation of endogenous astrocytic VRACs, we first employed a molecular genetics approach using *Nestin*$^{Cre}$-driven recombination. *Nestin*$^{Cre}$ targets neural precursor cells, leading to gene deletion in all cells of neuroectodermal origin, including astrocytes (62, 63). Our conditional knockout breeding strategy produced four genotypes: two types of controls (*Lrrc8a*$^{flox/+}$ and *Lrrc8a*$^{flox/flox}$ without Cre, referred to as fl/+ and fl/fl), a heterozygous (HET) LRRC8A deletion, and a homozygous LRRC8A knockout (KO) (Fig. 1A). Primary astrocyte cultures were prepared from neonatal brains of each genotype and successful Cre recombination was confirmed using the Ai9 tdTomato reporter. Live-cell imaging of tdTomato fluorescence showed complete Cre penetrance in both LRRC8A HET and KO astrocytes (representative images in Fig. 1B). Western blot analysis of astrocyte culture lysates revealed that heterozygous LRRC8A deletion reduced LRRC8A protein levels by approximately 60% ($p < 0.0001$, Fig. 1D), while KO cultures showed a complete loss of LRRC8A immunoreactivity ($p < 0.0001$, Fig. 1D, full western blot dataset in Supplemental Fig. S1).

*Insert Fig. 1 near here*

We next assessed functional VRAC activity using a D-[$^3$H]aspartate efflux assay. In control astrocytes, a 30% reduction in extracellular osmolality (to 200 mOsm) triggered a rapid increase in D-[$^3$H]aspartate release, reaching a peak rate of 2.6% within two minutes (an 8.7-fold rise over baseline), followed by a gradual decline consistent with the volume regulatory process. This kinetic profile closely matched our previous measurements of VRAC activation in both rat and mouse astrocytes (55, 59). Astrocytes with heterozygous LRRC8A deletion exhibited a 30% reduction in swelling-activated radiotracer efflux ($p = 0.038$, Fig. 1E, full analysis in Supplemental Fig. S2). As anticipated, LRRC8A KO astrocytes displayed a profound ~76% decrease in swelling-induced glutamate release ($p < 0.0001$, Fig. 1E and Supplemental Fig. S2). However, a small, transient release component persisted during the initial three minutes of hypoosmotic exposure (Fig. 1E). This residual response was characterized by more rapid activation and inactivation kinetics as compared to typical VRAC-mediated release and is likely mediated by a distinct mechanism (see additional considerations in the following paragraph and extended Discussion). Interestingly, LRRC8A KO astrocytes also showed a substantial reduction in baseline glutamate release under isoosmotic conditions: 28% lower than that of littermate controls ($p < 0.0001$ see inset in Fig. 1E). Together, these findings demonstrate that (i) LRRC8A containing VRACs are the primary conduit for swelling-induced glutamate release in astrocytes, and (ii) these channels also contribute to tonic glutamate release under resting, isoosmotic conditions.

To further investigate the apparent discrepancy between the 60% decrease in LRRC8A protein levels and the relatively modest 30% inhibition of swelling-activated glutamate release in HET cells, we performed additional functional assays using media with a more pronounced reduction in osmolality. When medium osmolality was decreased by ~50% (to 150 mOsm), VRAC activation was dramatically enhanced, compared to the response previously observed with a 30% (to 200mOsm) osmotic reduction, resulting in an over 10-fold increase in maximal release rates between the two conditions (compare Y-axis scales in Fig. 1E and 1F). LRRC8A KO cells again

321 showed a significant reduction in baseline glutamate release, a 40% decrease as compared to
322 controls ($p < 0.0001$, Fig. 1F, consistent with Fig. 1E). Importantly, in severely swollen astrocytes,
323 heterozygous LRRC8A deletion caused a much more pronounced 62% reduction in VRAC-
324 mediated activity, which is close to what would be expected based on changes in protein
325 expression in HET cells ($p < 0.0001$, Fig. 1F, full analysis in Supplemental Fig. S3). These results
326 may suggest that a reserve pool of LRRC8A-containing anion channels in the HET genotype can
327 compensate under moderate swelling conditions, but this compensatory capacity is lost with more
328 extreme osmotic stress/cellular swelling (see Discussion). This finding has implications for
329 interpreting subsequent RNAi-based knockdown experiments.

330 Finally, while comparing the "residual" D-[$^3$H]aspartate release in LRRC8A KO astrocytes
331 exposed to 30% and 50% reductions in medium osmolality, we found that the magnitude of this
332 release was indistinguishable between the two hypoosmotic conditions (maximal release rates:
333 0.62 ± 0.25% vs. 0.51 ± 0.32%, $p = 0.498$; insets in Fig. 1E and 1F). This was in stark contrast to
334 control astrocytes, in which VRAC activity increased by an order of magnitude under stronger
335 osmotic stress (2.59 ± 0.55% vs. 26.38 ± 5.19%, $p < 0.0001$). This lack of sensitivity to the extent
336 of cellular swelling further supports the conclusion that the residual release observed in LRRC8A
337 KO astrocytes is not mediated by VRAC (see Discussion). To explore alternative mechanism(s),
338 specifically, the contribution of $Ca^{2+}$-activated anion channels, we stimulated control and LRRC8A
339 KO astrocytes with the P2Y receptor agonist ATP (64). In these experiments, ATP triggered a
340 small, transient glutamate release with rapid inactivation kinetics (Supplemental Fig. S4). This
341 response partially resembled the "residual" glutamate release observed in LRRC8A KO
342 astrocytes under hypoosmotic conditions. Nevertheless, these results were inconclusive due to
343 the small amplitude and high variability of the ATP effects in both cell types.

344

## 345 Relative Abundance of *Lrrc8* Transcripts in Mouse Brain and Primary Astrocyte Cultures

346 We next measured and compared the endogenous expression of all five *Lrrc8* isoforms in
347 C57BL/6J mouse brains and primary astrocyte cultures derived from C57BL/6J neonates. qRT-
348 PCR analysis of samples prepared from forebrain tissue detected high levels of four *Lrrc8*
349 transcripts, *Lrrc8a-Lrrc8d*, with the order of abundance *Lrrc8b>Lrrc8a≈Lrrc8d>Lrrc8c* (Fig. 2A).
350 mRNA levels of the *Lrrc8* subunits were ~1-5% of the housekeeping gene ribosomal *Rpl13a*, or
351 0.5-2.5% of the highly prevalent *Gapdh* (Fig. 2A and Supplemental Fig. S5A). Consistent with
352 literature reports, brain levels of *Lrrc8e* were very low-to-non-detectable (Fig. 2A). To
353 independently validate our findings on *Lrrc8* expression, we additionally performed an in-silico
354 analysis of publicly available RNAseq datasets. Fig. 2B summarizes expression levels of the five
355 *Lrrc8* isoforms in seven forebrain regions from five mice of both sexes from the Human Protein
356 Atlas. The pattern of relative abundance of *Lrrc8* subunits in RNAseq datasets was nearly
357 identical to that found in our qRT-PCR experiments: *Lrrc8b>Lrrc8d≈Lrrc8a>Lrrc8c*, and extremely
358 low-to-nondetectable *Lrrc8e* (compare Fig. 2A and 2B).

359 For comparative purposes, we additionally analyzed *LRRC8* subunit expression in the
360 human brain using RNAseq datasets from the Genotype-Tissue Expression (GTEx) portal
361 [accessed on July 14, 2025]. To explore regional heterogeneity, we extracted expression data for
362 four forebrain regions: cortex, amygdala, caudate, and hippocampus (181-300 males and females
363 per region, Supplemental Fig. S6). Surprisingly, human tissue exhibited a strikingly different
364 *LRRC8* expression profile as compared to the mouse brain. In humans, *LRRC8A* dominated all
365 other LRRC8 subunits with up to 5-fold higher expression as compared to the next most abundant
366 isoform (Supplemental Fig. S6). The relative expression levels of human VRAC subunits were
367 *LRRC8A>>LRRC8B≈LRRC8D>>LRRC8C* (Supplemental Fig. S6, compare to mouse data in Fig.

368 2B). These species-specific differences should be considered when analyzing VRAC
369 stoichiometry, organization, and function across different organisms and model systems.

370 *Insert Fig. 2 near here*

371 Since our functional VRAC assays were performed in primary mouse astrocytes, we
372 further measured *Lrrc8* mRNA levels primary astrocyte cultures using qRT-PCR. In astrocyte
373 cultures, the average levels of *Lrrc8* transcripts were comparable to those observed in mouse
374 forebrain tissue. Expression levels of the four predominant *Lrrc8* isoforms ranged from ~1-4%
375 relative to *Rpl13a*, or 0.5-2% when normalized to *Gapdh* (Fig. 2C and Supplemental Fig. S5B).
376 As in brain tissue, *Lrrc8e* expression was detected at trace levels (Fig. 2C). Notably, we observed
377 cell type-specific differences in the relative expression of individual *Lrrc8* isoforms: cultured
378 astrocytes exhibited significantly higher levels of *Lrrc8c* and markedly lower levels of *Lrrc8b*
379 compared to brain tissue (compare Fig. 2A and Fig. 2C). These differences may reflect an intrinsic
380 cell type-specific *Lrrc8* expression profile or could result from artifacts introduced by *in vitro* culture
381 conditions.

382

383 **Validation of RNAi Approach for Probing VRAC Function**

384 To investigate the function of endogenous LRRC8 proteins in wild-type astrocytes, we
385 employed RNA interference (RNAi) using commercially available siRNA constructs. The temporal
386 dynamics and efficacy of siRNA-mediated knockdown were assessed by measuring LRRC8A
387 protein levels at 24-96h post-transfection with an *Lrrc8a*-targeting siRNA, termed siA1. LRRC8A
388 immunoreactivity declined progressively over time, with reductions of 46%, 87%, 93%, and 97%
389 at 24, 48, 72, and 96h, respectively (Fig. 3A, full western blot dataset in Supplemental Fig. S7).
390 Based on this time course, all subsequent functional assays were performed 96h after
391 transfection. The kinetics of protein loss suggested an LRRC8A half-life of approximately 24 h
392 (Fig. 3A).

393 *Insert Fig. 3 near here*

394 We next compared the efficacy of three independent *Lrrc8a*-targeting siRNAs, each
395 directed against distinct regions of the mRNA (siA1, siA3, and siA4; see Table 3). Ninety-six
396 hours post-transfection, all three constructs reduced LRRC8A protein levels by >90% ($p < 0.0001$;
397 Fig. 3B, full western blot dataset in Supplemental Fig. S8).

398 To determine the functional impact of siRNA-mediated LRRC8A depletion on VRAC
399 activity and compare it with genetic LRRC8A KO, we measured swelling-activated glutamate
400 release using a D-[$^3$H]aspartate efflux assay. Knockdown of LRRC8A significantly reduced D-
401 [$^3$H]aspartate efflux in response to a 30% reduction in medium osmolarity, with a ~65% decrease
402 in maximal release and ~57% decrease in area under the curve ($p < 0.0001$; Fig. 3C). The
403 magnitude of inhibition, 65% decrease, is comparable to the 76% reduction seen in LRRC8A KO
404 astrocytes (Fig. 1E), indicating that siRNA knockdown is highly effective. The residual VRAC
405 activity, despite near-total loss of detectable LRRC8A protein, likely reflects a non-proportional
406 relationship between protein abundance and channel function, or limitations in the sensitivity of
407 antibody-based detection.

408

409 **Analysis of Subunit-Specific Contributions of LRRC8B-E to Glutamate-Permeable VRACs**

410 To assess the individual contributions of all five LRRC8 isoforms to glutamate
411 permeability, we used an RNAi-based screening strategy. For each of the five *Lrrc8* mRNA
412 species, we tested three distinct siRNA constructs targeting different regions of the mRNA (see
413 Table 3 for target sequences). In cells treated with a non-targeting control siRNA (siNC), the

414 relative expression profile of *Lrrc8* transcripts remained unchanged (compare Fig. 2C and Fig.
415 4A1). All tested siRNA constructs achieved 70-90% knockdown of their respective targets (Fig.
416 4B1-F1). Therefore, all siRNA constructs were included in the initial functional screenings.

417 *Insert Fig. 4 near here*

418 To increase experimental throughput, initial VRAC activity assays were conducted in a
419 multi-well plate format, measuring swelling-activated D-[$^3$H]aspartate release in response to a
420 30% reduction in medium osmolarity (see schematic Fig. 4A2). As detailed in the Methods
421 section, these efflux assays were performed in $Na^+$-free medium to prevent reuptake of the tracer
422 by $Na^+$-dependent GLAST transporters. For all experiments, repeated-measures two-way
423 ANOVA revealed a main effect of medium osmolarity (basal vs. hypoosmotic; $p < 0.0001$),
424 consistent with VRAC activation (Fig. 4B2-F2). For simplicity, we present only post-hoc analyses
425 comparing the effects of individual siRNA constructs with those of siNC-treated controls under
426 hypoosmotic conditions. We first tested the effect of siRNA-mediated knockdown of the essential
427 LRRC8A subunit. All three siRNAs targeting LRRC8A (designated siA1, siA3, and siA4) strongly
428 reduced swelling-induced D-[$^3$H]aspartate release, decreasing it by 67-85% as compared to siNC
429 controls ($p < 0.0001$ vs. siNC; Fig. 4B2). The degree of inhibition ranked siA1 > siA3 > siA4 (Fig.
430 4B2). Importantly, the high inhibitory potency of the LRRC8A knockdown resembled the near-
431 complete loss of VRAC activity in LRRC8A KO astrocytes.

432 In contrast to the strong effect of LRRC8A knockdown, none of the siRNAs targeting
433 LRRC8B (siB1, siB3, and siB4) inhibited VRAC activity (Fig. 4C2). However, repeated measures
434 two-way ANOVA revealed a significant interaction between siRNA treatments and media
435 osmolarity ($p = 0.02$; Fig. 4C2), so we performed a post hoc analysis. Interestingly, one construct,
436 siB1, produced a statistically significant 24% increase in swelling-activated D-[$^3$H]aspartate
437 release ($p = 0.002$ vs. siNC; Fig. 4C2). For all subsequent experiments, we used siB4, which
438 demonstrated high efficacy in reducing *Lrrc8b* mRNA levels, without affecting functional VRAC
439 activity.

440 All three siRNA constructs targeting LRRC8C (siC1, siC2, and siC4) significantly reduced
441 VRAC activity ($p < 0.0001$ vs. siNC; Fig. 4D2). The most effective, siC1, reduced swelling-
442 activated D-[$^3$H]aspartate release by 56% ($p < 0.0001$ vs. siNC; Fig. 4D2). The order of inhibition
443 was siC1 > siC4 > siC2, which closely mirrored the efficacy of *Lrrc8c* mRNA knockdown (Fig.
444 4D1). Due to its superior efficacy, siC1 was used in all subsequent experiments. Western blotting
445 confirmed effective LRRC8C protein depletion at the time of functional analysis, with a ~79%
446 reduction in LRRC8C immunoreactivity 96h after siRNA transfection ($p < 0.0001$; Fig. 5A-B, full
447 western blot dataset in Supplemental Fig. S9). The prominent contribution of LRRC8C to VRAC-
448 mediated glutamate release in mouse astrocytes was surprising and contrasted with previous
449 reports in other cell types, including our own findings in rat astrocytes, which showed that
450 LRRC8C knockdown does not meaningfully impact swelling-activated D-[$^3$H]aspartate efflux (see
451 (55) and Discussion).

452 LRRC8D knockdowns produced more nuanced effects. Two of the tested siRNA
453 constructs, siD2 and siD4, reduced VRAC activity by 10% and 28%, respectively ($p = 0.542$ and
454 0.002 vs. siNC, Fig. 4E2). In contrast, siD1 produced a striking 60% increase in swelling-activated
455 D-[$^3$H]aspartate release ($p < 0.0001$ vs. siNC; Fig. 4E2). Follow-up qRT-PCR analysis revealed
456 that siD1 induced off-target effects, leading to a paradoxical upregulation of *Lrrc8a* and *Lrrc8c*
457 transcript levels by 2.5-fold and 1.7-fold, respectively (Supplemental Fig. S10). Based on its
458 superior efficacy and lack of off-target effects, siD4 was used in all subsequent experiments.
459 Western blotting showed a ~90% decrease in LRRC8D protein 96h post siRNA-transfection ($p <$
460 $0.0001$; Fig. 5C-D, full western blot dataset in Supplemental Fig. S11). Overall, these findings

461 suggest that LRRC8D plays a role in glutamate-permeable VRAC function, though its contribution
462 is relatively limited.

463 Finally, we tested three LRRC8E-targeting siRNA constructs (siE1, siE2, and siE4).
464 Although the LRRC8E subunit is expressed in mouse astrocytes at only trace levels (see Fig. 2C),
465 our prior work in rat astroglia has suggested that LRRC8E may be incorporated into astrocytic
466 VRACs and modulate swelling-activated glutamate release (55). In the current study, LRRC8E
467 knockdown had no biologically significant effect on VRAC activity in mouse astrocytes, albeit
468 small increases in VRAC activity were observed with all siRNA constructs ($p = 0.001$ vs. siNC,
469 Fig. 4F2).

470 *Insert Fig. 5 near here*

471

472 **siRNA Knockdown of LRRC8 Isoforms Modifies Protein Levels of Partnering Subunits**
473 **Without Affecting mRNA Expression**

474 To assess siRNA specificity and determine whether loss of individual LRRC8 subunits
475 influences the expression of the other family members, we performed qRT-PCR analysis of all
476 five *Lrrc8* transcripts in astrocytes transfected with the most effective siRNA constructs targeting
477 *Lrrc8a-d* (siA1, siB4, siC1, and siD4). At 48 hours post-transfection, knockdown of individual *Lrrc8*
478 subunits significantly altered only the targeted transcripts, without a strong effect on the remaining
479 *Lrrc8* genes (Fig. 6A-D). These results demonstrate the high specificity of this approach.

480 Given the established role of LRRC8A in membrane trafficking (24, 65), we next tested
481 whether manipulation of LRRC8A affects the protein stability of the other isoforms. Western blot
482 analysis of protein lysates from control (*Lrrc8a*$^{fl/+}$) and LRRC8A KO cultures revealed that
483 LRRC8A deletion significantly reduced LRRC8C and LRRC8D protein levels, with a more
484 pronounced effect on LRRC8C (>80% reduction, $p < 0.001$; Fig. 6E) compared with LRRC8D
485 (~40% reduction, $p < 0.001$; Fig. 6E, full western blot dataset in Supplemental Fig. S12).

486 The LRRC8A KO effects on LRRC8C and LRRC8D protein levels were partially recapitu-
487 lated in siA1-treated astrocytes. LRRC8A siRNA knockdown reduced LRRC8C protein levels by
488 64% ($p < 0.0001$, Fig. 6F) and LRRC8D levels by 42% (not significant, $p = 0.089$, Fig. 6F, full
489 western blot dataset in Supplemental Fig. S13). Altogether, these data show that both constitutive
490 deletion and siRNA-mediated knockdown of LRRC8A reduce the protein levels of the partnering
491 LRRC8C and LRRC8D subunits without altering their mRNA levels.

492 *Insert Fig. 6 near here*

493 To determine whether the regulation of protein stability is LRRC8A-specific, we tested the
494 effects of siRNA-mediated knockdowns of LRRC8C and LRRC8D. LRRC8C depletion reduced
495 LRRC8A immunoreactivity by ~74% ($p = 0.001$, Fig. 6G, full western blot dataset in Supplemental
496 Fig. S14). LRRC8D knockdown reduced LRRC8A protein levels by ~63% ($p = 0.002$, Fig. 6H, full
497 western blot dataset in Supplemental Fig. S15). In contrast, there was no strong mutual
498 interdependence between LRRC8C and LRRC8D. Specifically, LRRC8C knockdown had no
499 effect on LRRC8D ($p = 0.34$, Fig. 6G), and LRRC8D knockdown produced a ~40% decrease in
500 LRRC8C immunoreactivity, but this effect was not statistically significant ($p = 0.11$, Fig. 6H). The
501 pattern of selective co-stability of LRRC8 subunits supports the existence of distinct LRRC8A/C-
502 and LRRC8A/D-containing VRAC populations.

503

504 **Non-Redundant Functions of LRRC8C and LRRC8D in Glutamate-Permeable VRACs**

505 Although LRRC8C knockdown potently suppressed swelling-activated D-[$^3$H]aspartate

506 release (Fig. 4D2), the resulting inhibition was less pronounced than that observed after
507 knockdown of the essential LRRC8A (compare to Fig. 4B2). These findings may suggest that
508 other LRRC8 proteins function redundantly with LRRC8C in forming heteromeric VRACs. Our
509 early work established that, in rat astrocytes, LRRC8C and LRRC8D serve as mutually
510 replaceable partners of LRRC8A in forming glutamate-permeable VRACs (55). To test if this
511 redundancy extends to mouse astrocytes, we performed a double-knockdown of LRRC8C and
512 LRRC8D.

513 We first verified that co-transfection with siRNAs targeting *Lrrc8c* (siC1) and *Lrrc8d* (siD4)
514 effectively reduced target gene expression by ≥80%, both individually and in combination (Fig.
515 7A). Functional assays performed in a multi-well plate revealed that dual knockdown of LRRC8C
516 and LRRC8D did not further decrease glutamate release as compared to LRRC8C knockdown
517 alone (57% vs. 52% inhibition, $p = 0.240$, Fig. 7B). To assess VRAC activity with higher temporal
518 resolution, we repeated the double-knockdown experiments using a Lucite superfusion system.
519 In this format, LRRC8C knockdown significantly reduced the maximum rate of glutamate release
520 by ~40% ($p < 0.0001$, Fig. 7C), whereas LRRC8D knockdown produced a smaller, non-significant
521 ~20% decrease ($p = 0.084$, Fig. 7C). Combined knockdown of LRRC8C+D inhibited VRAC activity
522 by ~48% ($p < 0.001$, Fig. 7C); however, this effect was not significantly different from LRRC8C
523 knockdown alone ($p = 0.688$; Fig. 7C). Consistent with this finding, analysis of the integral VRAC-
524 mediated release under hypoosmotic conditions showed no significant difference between siC1
525 alone and the siC1+siD4 combination ($p = 0.603$, Fig. 7C). While differences in the degree of
526 VRAC inhibition between plate-based and superfusion formats were observed, the lack of an
527 additive effect between LRRC8C and LRRC8D knockdowns was consistent across both assays.

528 *Insert Fig. 7 near here*

529 Our LRRC8A KO data, particularly the heterozygous LRRC8A deletion results, suggest
530 that in cells exposed to a 30% reduction in medium osmolality, VRAC channels may retain spare
531 capacity, obscuring the full effects of LRRC8 subunit knockdown. Therefore, we repeated the
532 double-knockdown experiments in astrocytes exposed to a 50% reduction in medium osmolarity
533 (Fig. 7D). Under these conditions, knockdown of individual LRRC8C and LRRC8D subunits
534 strongly inhibited VRAC activity (~53% and ~41% decrease in maximal release rates,
535 respectively; $p < 0.0001$ vs. siNC, Fig. 7D). The double knockdown of LRRC8C plus LRRC8D
536 produced partially additive ~72% inhibition ($p = 0.004$, vs LRRC8C knockdown and $p = 0.0001$
537 vs. LRRC8D depletion alone, Fig. 7D). Partial additivity of the double-knockdown (as opposed to
538 synergistic effect) is consistent with the existence of separate LRRC8A+LRRC8C and LRRC8A+
539 LRRC8D-containing heteromeric VRACs (see Discussion).

540

541 **LRRC8B Downregulation Rescues the Effects of LRRC8C- and LRRC8D-Knockdowns on**
542 **VRAC Activity**

543 Given that the combined downregulation of LRRC8C and LRRC8D did not reach the full
544 effect of LRRC8A knockdown, we hypothesized that another abundant LRRC8 isoform, namely
545 LRRC8B, serves as a functional substitute for either LRRC8C and/or LRRC8D. To test this
546 hypothesis, we explored the potential contribution of LRRC8B in double-knockdown siRNA
547 assays. Our prediction was that knocking down either LRRC8C+LRRC8B or LRRC8D+LRRC8B
548 would produce a more substantial functional effect than knocking down LRRC8C or LRRC8D
549 alone.

550 We first validated the specificity and efficacy of the double-knockdown of LRRC8B and
551 LRRC8C. qRT-PCR analysis confirmed that siB4 and siC1 constructs were equally effective when
552 transfected alone or in combination (Fig. 8A). Unexpectedly, in functional VRAC assays, the

553 double knockdown of LRRC8B and LRRC8C resulted in a partial rescue of VRAC-mediated
554 glutamate release as compared to the effect of LRRC8C knockdown on its own (Fig. 8B).
555 Specifically, the siB4 construct had no effect ($p = 0.98$; Fig. 8B), siC1 suppressed VRAC activity
556 by 51% ($p < 0.0001$; Fig. 8B), and the combination of siB4 and siC1 paradoxically caused a
557 smaller 25% inhibition ($p < 0.0001$, siB1+C1 vs. siC1 alone, Fig. 8B). This functional rescue
558 appears to be independent of protein stability given that LRRC8B knockdown caused a ~27%
559 reduction in LRRC8C protein ($p = 0.044$, Fig. 8C) and had no effect on LRRC8A ($p = 0.641$,
560 Supplemental Fig. S16).

561 *Insert Fig. 8 near here*

562 Similarly, we quantified the efficacy of double-knockdown of LRRC8B and LRRC8D. qRT-
563 PCR analysis verified that siB4 and siD4 constructs were equally effective when transfected alone
564 or in combination (Fig. 8D). In functional assays, the double knockdown of LRRC8B and LRRC8D
565 resulted in a complete rescue of the VRAC-mediated glutamate release as compared to the effect
566 LRRC8D knockdown on its own (Fig. 8E). Specifically, siB4 had no effect ($p = 0.415$; Fig. 8E),
567 siD4 reduced VRAC activity by 17% ($p < 0.001$; Fig. 8E), and the combination of siB4 and siD4
568 caused full recovery of glutamate release in hypoosmotic medium ($p = 0.36$, Fig. 8E). In
569 complementary Western blot analysis, we found no effects of LRRC8B knockdown on LRRC8D
570 protein levels ($p = 0.717$, Fig. 8F, full western blot dataset in Supplemental Fig. S17).

571 It is important to note that the rescue effects of co-transfection with siB4 were subunit
572 specific. In experiments involving the combined knockdown of LRRC8A+LRRC8B, the effect of
573 siA1+siB4 was no different from the effect of siA1 alone (Supplemental Fig. S18A). Overall, these
574 data suggest that LRRC8B may act as a structural partner within LRRC8A+LRRC8C and
575 LRRC8A+LRRC8D-containing channels.

576

577 # DISCUSSION

578

579 The main objective of this study was to identify which LRRC8 isoforms contribute to the
580 formation of glutamate-permeable VRACs in mouse astrocytes. Our key findings can be
581 summarized as follows: (1) Genetic knockout of the essential LRRC8A subunit confirmed that
582 LRRC8A-containing VRACs are the primary pathway for astrocytic swelling-activated glutamate
583 release and account for ~98% of the release under conditions of substantial cell swelling. (2) RNAi
584 analysis supported a model in which glutamate-permeable VRACs strongly depend on LRRC8A
585 and LRRC8C. Interestingly, LRRC8A and LRRC8C are reciprocally required for the protein
586 stability of their partner subunit, without affecting their mRNA levels. (3) The LRRC8D isoform
587 provided an additional contribution to swelling-activated glutamate release, but is likely present in
588 a distinct subpopulation of VRACs. This model is supported by both functional glutamate release
589 assays and the lack of mutual regulation of LRRC8C and LRRC8D protein stability.

590 Despite extensive work in the field, it remains debated whether VRACs are the primary
591 pathway for swelling-activated glutamate release in astrocytes. Several alternative mechanisms
592 have been proposed, including swelling-activated SLCO2A1-containing Maxi $Cl^-$ channels (66,
593 67), the Tweety homolog proteins TTYH1-3 (68), and $Ca^{2+}$-activated BEST1 channels (69, 70).
594 Furthermore, astroglial Cx43 hemichannels (71) and the $P2X_7$ receptor-activated pannexin
595 complexes (72, 73) can also release amino acid gliotransmitters in response to various stimuli.
596 Consistent with our prior work (30), genetic deletion of the essential VRAC subunit LRRC8A
597 largely abolished swelling-activated glutamate release. A small, swelling-independent residual

598 component persisted in LRRC8A-null cells, likely mediated by an alternative pathway(s) or cell
599 lysis, but its quantitative contribution appeared minimal. LRRC8A KO astrocytes also showed
600 reduced basal glutamate release under isoosmotic conditions, indicating tonic VRAC activity in
601 non-swollen cells. Interestingly, heterozygous LRRC8A deletion produced only a mild inhibition
602 of glutamate release in astrocytes exposed to a 30% reduction in medium osmolarity [this study
603 and (30)], but strongly suppressed glutamate efflux when cells were subjected to more
604 substantial, supraphysiological cell swelling. One interpretation of these findings is that severe
605 swelling activates the full complement of VRACs in the plasma membrane and recruits additional
606 channels from intracellular organellar reserves, unmasking the maximal functional deficit.
607 Together, these findings indicate that LRRC8A-containing VRACs dominate swelling-activated
608 glutamate release and contribute to tonic glutamate efflux in non-swollen astrocytes.

609 The subunit composition of VRACs that conduct organic anions, particularly glutamate
610 and aspartate, remains uncertain. Model biophysical studies have produced somewhat conflicting
611 results. In CRISPR/Cas9-edited LRRC8-null HEK293 cells, heterologous co-expression of
612 LRRC8A with LRRC8D or LRRC8A with LRRC8E produced glutamate-permeable VRACs,
613 whereas complexes of LRRC8A+LRRC8C showed limited glutamate conductance (54). In
614 comparison, in *Xenopus* oocytes, co-expression of LRRC8A with LRRC8C or LRRC8A with
615 LRRC8E resulted in significant glutamate permeability, whereas LRRC8A+LRRC8D heteromers
616 yielded smaller glutamate conductance (56). In native environments, VRACs are thought to
617 contain multiple, functionally redundant LRRC8 subunits, since deletion of individual LRRC8B-E
618 proteins failed to reduce endogenous VRAC currents in HEK293 or HeLa cells (24, 74).
619 Consistent with this idea, we previously reported that, in rat astrocytes, endogenous glutamate-
620 permeable VRACs are formed with redundant contributions from LRRC8C, LRRC8D, and
621 LRRC8E (55). Within this context, we were surprised to find that in mouse astroglia, swelling-
622 activated glutamate release strongly depended on LRRC8C expression, with 56% inhibition of
623 glutamate release following individual LRRC8C knockdown. In contrast, downregulation of
624 LRRC8D produced only a mild reduction in swelling-activated glutamate release, suggesting a
625 more limited role for this isoform. Recent studies further highlight the importance of LRRC8C,
626 demonstrating loss of VRAC currents in LRRC8C-null mouse T lymphocytes and marked
627 inhibition of VRAC currents after LRRC8C knockdown in human umbilical endothelial cells (75,
628 76).

629 *Insert Fig. 9 near here*

630 Given that depletion of either LRRC8C or LRRC8D alone failed to reproduce the strong
631 inhibition observed after loss of LRRC8A, we next examined whether combined LRRC8C+
632 LRRC8D knockdown produced additive or synergistic inhibition. A synergistic effect, as previously
633 reported in rat astrocytes (55), would support redundant contributions of LRRC8C and LRRC8D
634 within a single heteromeric VRAC. Alternatively, additive effects would favor the existence of two
635 distinct channel populations. In moderately swollen cells, combined knockdown of LRRC8C and
636 LRRC8D did not further inhibit glutamate release beyond that observed with LRRC8C depletion
637 alone (Fig. 9). The clear absence of synergism argues against a single-channel model. Although
638 the lack of additivity introduces some uncertainty, the glutamate release data are generally
639 consistent with a two-channel model. The idea of two independent channels is further supported
640 by the analysis of subunit-specific regulation of LRRC8 protein stability. We found strong
641 reciprocal regulation between LRRC8A and LRRC8C, as well as between LRRC8A and LRRC8D.
642 In contrast, we found minimal cross-regulation between LRRC8C and LRRC8D. The surprising
643 interdependence of LRRC8 subunit stability has a recent precedent in the mouse endothelium,

644 where LRRC8A, LRRC8B, and LRRC8C all mutually regulate the protein abundance of their
645 partnering isoforms (76). We speculate that loss of a given VRAC subunit promotes degradation
646 of its partners within the same channel complex, and the lack of co-dependence between
647 LRRC8C and LRRC8D points to their presence in distinct VRAC assemblies.

648 Interestingly, the relative impact of LRRC8D depletion on swelling-activated glutamate
649 release is substantially increased in astrocytes subjected to supraphysiological cell swelling,
650 induced by a 50% reduction in medium osmolarity. In this instance, the combined knockdown of
651 LRRC8C and LRRC8D produced nearly additive inhibition, consistent with a two-population
652 model. The increased role of LRRC8D during severe cell swelling may reflect recruitment of
653 additional LRRC8D-containing channels to the plasma membrane. In support of this idea, Groulx
654 et al. reported that mammalian cells accommodated moderate cell volume increases primarily
655 through shape changes, whereas in substantially swollen cells, membrane tension was compen-
656 sated for by endomembrane insertion (77). While the organellar distribution of VRACs is
657 incompletely understood, a substantial fraction of LRRC8 channels are thought to reside in the
658 lysosomal compartment and are recruited to the plasmalemma in response to severe
659 hypoosmotic stress (78). Also of importance, a recent study demonstrated that native lysosomal
660 VRACs are composed of LRRC8A, LRRC8B, LRRC8D, and LRRC8E subunits, with a notable
661 absence of LRRC8C (79). Thus, mobilization from intracellular pools is likely to preferentially
662 enrich the surface expression of LRRC8D-containing VRACs.

663 Finally, we would like to address the functional role of LRRC8B, which is highly expressed
664 in the mouse brain [(25) and present data]. In mouse astrocytes, LRRC8B knockdown alone did
665 not inhibit swelling-activated glutamate release. However, the combined downregulation of
666 LRRC8B in conjunction with LRRC8C or LRRC8D partially rescued the inhibitory effects of
667 LRRC8C or LRRC8D depletion alone. Similar paradoxical observations have been reported in
668 HEK293 cells, where deletion of LRRC8B from native VRACs increased swelling-activated D-
669 [$^3$H]aspartate efflux (54). Although the LRRC8B subunit can be incorporated into VRACs (24, 76),
670 its relevance to VRAC activity remains unclear. To date, the only established role for LRRC8B is
671 the modulation of $Ca^{2+}$ leak from the endoplasmic reticulum (80). Heterologous co-expression of
672 LRRC8A and LRRC8B fails to produce functional VRAC currents (24, 54, 56, 74). It is known that
673 homomeric LRRC8A channels have little to no conductance due to steric restrictions, including
674 the ring of positively charged arginine residues (R103) within the narrowest region of the pore
675 (47-49). LRRC8B shares structural homology with LRRC8A and contains a matching arginine
676 residue (R99), whereas LRRC8C-E have neutral amino acids at this position (47, 48, 50, 81). We
677 speculate that substituting LRRC8B for LRRC8C or LRRC8D within VRAC heteromers partially
678 narrows the channel pore, and that, in the double knockdown experiments, removing LRRC8B
679 makes the residual VRACs more permeable to glutamate. It is also possible that LRRC8B
680 knockdown effects may stem from modified intracellular $Ca^{2+}$ signaling.

681 In summary, our findings establish that glutamate permeability of native VRACs in mouse
682 astrocytes is largely determined by the non-redundant contributions of two subunits: the essential
683 LRRC8A and the complementary LRRC8C. This refined understanding of VRAC composition in
684 the brain has broad clinical relevance, given that both loss and gain of VRAC function produce
685 severe neurological phenotypes in humans. For example, gain-of-function mutations in *LRRC8C*
686 cause a severe multisystem disorder, termed *LRRC8C*-related TIMES syndrome, which is
687 associated with microcephaly, intellectual disability, and seizures (82). Conversely, mutations
688 causing megalencephalic leukoencephalopathy with subcortical cysts (MLC) indirectly reduce

689 VRAC activity and cause macrocephaly, white-matter disorganization, and severe seizures (83-
690 85). These neurological manifestations may, at least in part, be due to altered neurotransmitter
691 release via VRACs. Defining the structural determinants that govern VRAC neurotransmitter
692 permeability, therefore, provides critical insight into brain (patho)physiology and may guide the
693 development of subunit-targeted VRAC therapies.

694 ## DATA AVAILABILITY

695 All primary data included in this manuscript have been archived in the Open Science Framework
696 depository (osf.io) and can be accessed at https://osf.io/xvyba. All original Western blot images
697 are available in FigShare at https://doi.org/10.6084/m9.figshare.31143022

698

699 ## SUPPLEMENTAL MATERIAL

700 Supplemental Figs. S1-S18: https://doi.org/10.6084/m9.figshare.31143022

701

702 ## ACKNOWLEDGMENTS

703 The authors thank Dr. Preeti Dohare for help with validating LRRC8D siRNA constructs, Dr. Alena
704 Rudkouskya for help with LRRC8A Western blot experiments, and Antonio M. Fidaleo for his
705 advice on performing RNA-seq analyses. Illustrations in Figs. 2, 4, 9, and Graphical Abstract have
706 been created with BioRender.

707

708 ## GRANTS

709 This study was supported by the National Institutes of Health, grants R01 NS111943 and R21
710 NS140782 (to A.A.M.).

711

712 ## DISCLOSURES

713 The authors have no conflict of interest, financial or otherwise, to disclose.

714

715 ## AUTHOR CONTRIBUTIONS

716 Conceived and designed research: M.L.C. and A.A.M. Performed experiments: M.L.C., A.D.S.,
717 J.W.N. Analyzed data: M.L.C., A.D.S., A.A.M. Interpreted results: M.L.C. and A.A.M. Prepared
718 figures: M.L.C. and A.A.M. Drafted manuscript: M.L.C. and A.A.M. Edited and revised manuscript,
719 M.L.C., A.D.S., J.W.N., and A.A.M. Approved final version of manuscript: M.L.C., A.D.S., J.W.N.,
720 and A.A.M.

721

722 # REFERENCES
723


724 1. **Strange K, Emma F and Jackson PS**. Cellular and molecular physiology of volume-sensitive anion
725 channels. *Am J Physiol* 270: C711-C730, 1996.

726 2. **Okada Y**. Volume expansion-sensing outward-rectifier Cl- channel: fresh start to the molecular
727 identity and volume sensor. *Am J Physiol* 273: C755-C789, 1997. doi:
728 10.1152/ajpcell.1997.273.3.C755

729 3. **Nilius B, Eggermont J, Voets T, Buyse G, Manolopoulos V and Droogmans G**. Properties of
730 volume-regulated anion channels in mammalian cells. *Prog Biophys Mol Biol* 68: 69-119, 1997.

731 4. **Hazama A and Okada Y**. Ca2+ sensitivity of volume-regulatory K+ and Cl- channels in cultured
732 human epithelial cells. *J Physiol* 402: 687-702, 1988.

733 5. **Cahalan MD and Lewis RS**. Role of potassium and chloride channels in volume regulation by T
734 lymphocytes. *Soc Gen Physiol Ser* 43: 281-301, 1988. doi: n/a

735 6. **Worrell RT, Butt AG, Cliff WH and Frizzell RA**. A volume-sensitive chloride conductance in
736 human colonic cell line T84. *Am J Physiol* 256: C1111-C1119, 1989.

737 7. **Solc CK and Wine JJ**. Swelling-induced and depolarization-induced Cl- channels in normal and
738 cystic fibrosis epithelial cells. *Am J Physiol* 261: C658-C674, 1991. doi:
739 10.1152/ajpcell.1991.261.4.C658

740 8. **Kimelberg HK, Goderie SK, Higman S, Pang S and Waniewski RA**. Swelling-induced release of
741 glutamate, aspartate, and taurine from astrocyte cultures. *J Neurosci* 10: 1583-1591, 1990.

742 9. **Roy G and Malo C**. Activation of amino acid diffusion by a volume increase in cultured kidney
743 (MDCK) cells. *J Membr Biol* 130: 83-90, 1992.

744 10. **Kirk K, Ellory JC and Young JD**. Transport of organic substrates via a volume-activated channel. *J*
745 *Biol Chem* 267: 23475-23478, 1992.

746 11. **Jackson PS and Strange K**. Volume-sensitive anion channels mediate swelling-activated inositol
747 and taurine efflux. *Am J Physiol* 265: C1489-C1500, 1993. doi: 10.1152/ajpcell.1993.265.6.C1489

748 12. **Lang F, Busch GL, Ritter M, Volkl H, Waldegger S, Gulbins E and Haussinger D**. Functional
749 significance of cell volume regulatory mechanisms. *Physiol Rev* 78: 247-306, 1998.

750 13. **Hoffmann EK, Lambert IH and Pedersen SF**. Physiology of cell volume regulation in vertebrates.
751 *Physiol Rev* 89: 193-277, 2009.

752 14. **Eggermont J, Trouet D, Carton I and Nilius B**. Cellular function and control of volume-regulated
753 anion channels. *Cell Biochem Biophys* 35: 263-274, 2001.

754 15. **Mongin AA**. Volume-regulated anion channel--a frenemy within the brain. *Pflugers Arch* 468:
755 421-441, 2016.

756 16. **Jentsch TJ**. VRACs and other ion channels and transporters in the regulation of cell volume and
757 beyond. *Nat Rev Mol Cell Biol* 17: 293-307, 2016.

758 17. **Chen L, Konig B, Liu T, Pervaiz S, Razzaque YS and Stauber T**. More than just a pressure relief
759 valve: physiological roles of volume-regulated LRRC8 anion channels. *Biol Chem* 400: 1481-1496,
760 2019. doi: 10.1515/hsz-2019-0189

761 18. **Okada Y**. Physiology of the volume-sensitive/regulatory anion channel VSOR/VRAC: part 2: its
762 activation mechanisms and essential roles in organic signal release. *J Physiol Sci* 74: 34, 2024.
763 doi: 10.1186/s12576-023-00897-x

764 19. **Thone FMB, Polovitskaya MM and Jentsch TJ**. LRRC8/VRAC chloride and metabolite channels in
765 signaling and volume regulation. *Trends Biochem Sci* 50: 873-891, 2025. doi:
766 10.1016/j.tibs.2025.07.001

767 20. **Pedersen SF, Okada Y and Nilius B**. Biophysics and physiology of the volume-regulated anion
768 channel (VRAC)/volume-sensitive outwardly rectifying anion channel (VSOR). *Pflugers Arch* 468:
769 371-383, 2016.

770 21. **Strange K, Yamada T and Denton JS**. A 30-year journey from volume-regulated anion currents
771 to molecular structure of the LRRC8 channel. *J Gen Physiol* 151: 100-117, 2019.

772 22. **Okada Y**. Physiology of the volume-sensitive/regulatory anion channel VSOR/VRAC. Part 1: from
773 its discovery and phenotype characterization to the molecular entity identification. *J Physiol Sci*
774 74: 3, 2024. doi: 10.1186/s12576-023-00897-x

775 23. **Qiu Z, Dubin AE, Mathur J, Tu B, Reddy K, Miraglia LJ, Reinhardt J, Orth AP and Patapoutian A**.
776 SWELL1, a plasma membrane protein, is an essential component of volume-regulated anion
777 channel. *Cell* 157: 447-458, 2014.

778 24. **Voss FK, Ullrich F, Munch J, Lazarow K, Lutter D, Mah N, Andrade-Navarro MA, von Kries JP,**
779 **Stauber T and Jentsch TJ**. Identification of LRRC8 heteromers as an essential component of the
780 volume-regulated anion channel VRAC. *Science* 344: 634-638, 2014. doi:
781 10.1126/science.1252826

782 25. **Abascal F and Zardoya R**. LRRC8 proteins share a common ancestor with pannexins, and may
783 form hexameric channels involved in cell-cell communication. *Bioessays* 34: 551-560, 2012.

784 26. **Kumar L, Chou J, Yee CS, Borzutzky A, Vollmann EH, von Andrian UH, Park SY, Hollander G,**
785 **Manis JP, Poliani PL and Geha RS**. Leucine-rich repeat containing 8A (LRRC8A) is essential for T
786 lymphocyte development and function. *J Exp Med* 211: 929-942, 2014.

787 27. **Zhang Y, Xie L, Gunasekar SK, Tong D, Mishra A, Gibson WJ, Wang C, Fidler T, Marthaler B,**
788 **Klingelhutz A, Abel ED, Samuel I, Smith JK, Cao L and Sah R**. SWELL1 is a regulator of adipocyte
789 size, insulin signalling and glucose homeostasis. *Nat Cell Biol* 19: 504-517, 2017.

790 28. **Yang J, Vitery MDC, Chen J, Osei-Owusu J, Chu J and Qiu Z**. Glutamate-releasing SWELL1
791 channel in astrocytes modulates synaptic transmission and promotes brain damage in stroke.
792 *Neuron* 102: 813-827, 2019. doi: 10.1016/j.neuron.2019.03.029

793 29. **Kumar A, Xie L, Ta CM, Hinton AO, Gunasekar SK, Minerath RA, Shen K, Maurer JM, Grueter**
794 **CE, Abel ED, Meyer G and Sah R**. SWELL1 regulates skeletal muscle cell size, intracellular
795 signaling, adiposity and glucose metabolism. *eLife* 9: 2020.

796 30. **Wilson CS, Dohare P, Orbeta S, Nalwalk JW, Huang Y, Ferland RJ, Sah R, Scimemi A and Mongin**
797 **AA**. Late adolescence mortality in mice with brain-specific deletion of the volume-regulated
798 anion channel subunit LRRC8A. *FASEB J* 35: e21869, 2021. doi: 10.1096/fj.202002745R

799 31. **Zhou JJ, Luo Y, Chen SR, Shao JY, Sah R and Pan HL**. LRRC8A-dependent volume-regulated anion
800 channels contribute to ischemia-induced brain injury and glutamatergic input to hippocampal
801 neurons. *Exp Neurol* 332: 113391, 2020.

802 32. **Kimelberg HK, MacVicar BA and Sontheimer H**. Anion channels in astrocytes: Biophysics,
803 pharmacology, and function. *Glia* 54: 747-757, 2006.

804 33. **Akita T and Okada Y**. Characteristics and roles of the volume-sensitive outwardly rectifying
805 (VSOR) anion channel in the central nervous system. *Neuroscience* 275: 211-231, 2014.

806 34. **Wilson CS and Mongin AA**. Cell volume control in healthy brain and neuropathologies. *Curr Top*
807 *Membr* 81: 385-455, 2018.

808 35. **Kimelberg HK**. Astrocytic swelling in cerebral ischemia as a possible cause of injury and target
809 for therapy. *Glia* 50: 389-397, 2005.

810 36. **Mongin AA**. Disruption of ionic and cell volume homeostasis in cerebral ischemia: The perfect
811 storm. *Pathophysiology* 14: 183-193, 2007.

812 37. **Mongin AA and Kimelberg HK**. ATP potently modulates anion channel-mediated excitatory
813 amino acid release from cultured astrocytes. *Am J Physiol Cell Physiol* 283: C569-C578, 2002.

814 38. **Takano T, Kang J, Jaiswal JK, Simon SM, Lin JH, Yu Y, Li Y, Yang J, Dienel G, Zielke HR and**
815 **Nedergaard M**. Receptor-mediated glutamate release from volume sensitive channels in
816 astrocytes. *Proc Natl Acad Sci U S A* 102: 16466-16471, 2005.

817 39. **Liu HT, Akita T, Shimizu T, Sabirov RZ and Okada Y**. Bradykinin-induced astrocyte-neuron
818 signalling: glutamate release is mediated by ROS-activated volume-sensitive outwardly rectifying
819 anion channels. *J Physiol* 587: 2197-2209, 2009.

820 40. **Yang J, Chen J, Liu Y, Chen KH, Baraban JM and Qiu Z**. Ventral tegmental area astrocytes
821 modulate cocaine reward by tonically releasing GABA. *Neuron* 111: 1104-1117, 2023. doi:
822 10.1016/j.neuron.2022.12.033

823 41. **Kimelberg HK, Feustel PJ, Jin Y, Paquette J, Boulos A, Keller RW, Jr. and Tranmer BI**. Acute
824 treatment with tamoxifen reduces ischemic damage following middle cerebral artery occlusion.
825 *Neuroreport* 11: 2675-2679, 2000.

826 42. **Kimelberg HK, Jin Y, Charniga C and Feustel PJ**. Neuroprotective activity of tamoxifen in
827 permanent focal ischemia. *J Neurosurg* 99: 138-142, 2003.

828 43. **Zhang Y, Zhang H, Feustel PJ and Kimelberg HK**. DCPIB, a specific inhibitor of volume regulated
829 anion channels (VRACs), reduces infarct size in MCAo and the release of glutamate in the
830 ischemic cortical penumbra. *Exp Neurol* 210: 514-520, 2008.

831 44. **Boulos AS, Deshaies EM, Dalfino JC, Feustel PJ, Popp AJ and Drazin D**. Tamoxifen as an effective
832 neuroprotectant in an endovascular canine model of stroke. *J Neurosurg* 114: 1117-1126, 2011.

833 45. **Chen J, Yang J, Chu J, Chen KH, Alt J, Rais R and Qiu Z**. The SWELL1 channel promotes ischemic
834 brain damage by mediating neuronal swelling and glutamate toxicity. *Adv Sci (Weinh )* 11:
835 e2401085, 2024. doi: 10.1002/advs.202401085

836 46. **Balkaya M, Dohare P, Chen S, Schober AL, Fidaleo AM, Nalwalk JW, Sah R and Mongin AA**.
837 Conditional deletion of LRRC8A in the brain reduces stroke damage independently of swelling-
838 activated glutamate release. *iScience* 26: 106669, 2023. doi: 10.1016/j.isci.2023.106669

839 47. **Deneka D, Sawicka M, Lam AKM, Paulino C and Dutzler R**. Structure of a volume-regulated
840 anion channel of the LRRC8 family. *Nature* 558: 254-259, 2018.

841 48. **Kasuya G, Nakane T, Yokoyama T, Jia Y, Inoue M, Watanabe K, Nakamura R, Nishizawa T,**
842 **Kusakizako T, Tsutsumi A, Yanagisawa H, Dohmae N, Hattori M, Ichijo H, Yan Z, Kikkawa M,**
843 **Shirouzu M, Ishitani R and Nureki O**. Cryo-EM structures of the human volume-regulated anion
844 channel LRRC8. *Nat Struct Mol Biol* 25: 797-804, 2018.

845 49. **Kefauver JM, Saotome K, Dubin AE, Pallesen J, Cottrell CA, Cahalan SM, Qiu Z, Hong G,**
846 **Crowley CS, Whitwam T, Lee WH, Ward AB and Patapoutian A**. Structure of the human volume
847 regulated anion channel. *eLife* 7: e38461, 2018.

848 50. **Kern DM, Oh S, Hite RK and Brohawn SG**. Cryo-EM structures of the DCPIB-inhibited volume-
849 regulated anion channel LRRC8A in lipid nanodiscs. *eLife* 8: e42636, 2019. doi:
850 10.7554/eLife.42636

851 51. **Rutz S, Deneka D, Dittmann A, Sawicka M and Dutzler R**. Structure of a volume-regulated
852 heteromeric LRRC8A/C channel. *Nat Struct Mol Biol* 30: 52-61, 2023.

853 52. **Lurie A, Stephens CA, Kern DM, Henn KM, Latorraca NR and Brohawn SG**. Assembly and lipid-
854 gating of LRRC8A:D volume-regulated anion channels. *Nat Commun* 17: 366, 2026. doi:
855 10.1038/s41467-025-67052-5

856 53. **Planells-Cases R, Lutter D, Guyader C, Gerhards NM, Ullrich F, Elger DA, Kucukosmanoglu A, Xu**
857 **G, Voss FK, Reincke SM, Stauber T, Blomen VA, Vis DJ, Wessels LF, Brummelkamp TR, Borst P,**
858 **Rottenberg S and Jentsch TJ**. Subunit composition of VRAC channels determines substrate
859 specificity and cellular resistance to Pt-based anti-cancer drugs. *EMBO J* 34: 2993-3008, 2015.
860 doi: 10.15252/embj.201592409

861 54. **Lutter D, Ullrich F, Lueck JC, Kempa S and Jentsch TJ**. Selective transport of neurotransmitters
862 and modulators by distinct volume-regulated LRRC8 anion channels. *J Cell Sci* 130: 1122-1133,
863 2017. doi: 10.1242/jcs.196253

864 55. **Schober AL, Wilson CS and Mongin AA**. Molecular composition and heterogeneity of the LRRC8-
865 containing swelling-activated osmolyte channels in primary rat astrocytes. *J Physiol* 595: 6939-
866 6951, 2017. doi: 10.1113/JP275053

867 56. **Gaitan-Penas H, Gradogna A, Laparra-Cuervo L, Solsona C, Fernandez-Duenas V, Barrallo-**
868 **Gimeno A, Ciruela F, Lakadamyali M, Pusch M and Estevez R**. Investigation of LRRC8-mediated
869 volume-regulated anion currents in Xenopus oocytes. *Biophys J* 111: 1429-1443, 2016. doi:
870 10.1016/j.bpj.2016.08.030

871 57. **Livak KJ and Schmittgen TD**. Analysis of relative gene expression data using real-time
872 quantitative PCR and the 2(-Delta Delta C(T)) Method. *Methods* 25: 402-408, 2001.

873 58. **Schneider CA, Rasband WS and Eliceiri KW**. NIH Image to ImageJ: 25 years of image analysis.
874 *Nat Methods* 9: 671-675, 2012.

875 59. **Abdullaev IF, Rudkouskaya A, Schools GP, Kimelberg HK and Mongin AA**. Pharmacological
876 comparison of swelling-activated excitatory amino acid release and Cl- currents in rat cultured
877 astrocytes. *J Physiol* 572: 677-689, 2006. doi: 10.1113/jphysiol.2005.103820

878 60. **Bowens NH, Dohare P, Kuo YH and Mongin AA**. DCPIB, the proposed selective blocker of
879 volume-regulated anion channels, inhibits several glutamate transport pathways in glial cells.
880 *Mol Pharmacol* 83: 22-32, 2013. doi: 10.1124/mol.112.080457

881 61. **Schober AL and Mongin AA**. Intracellular levels of glutamate in swollen astrocytes are preserved
882 via neurotransmitter reuptake and de novo synthesis: implications for hyponatremia. *J*
883 *Neurochem* 135: 176-185, 2015. doi: 10.1111/jnc.13229

884 62. **Tronche F, Kellendonk C, Kretz O, Gass P, Anlag K, Orban PC, Bock R, Klein R and Schutz G**.
885 Disruption of the glucocorticoid receptor gene in the nervous system results in reduced anxiety.
886 *Nat Genet* 23: 99-103, 1999. doi: 10.1038/12703

887 63. **Dubois NC, Hofmann D, Kaloulis K, Bishop JM and Trumpp A**. Nestin-Cre transgenic mouse line
888 Nes-Cre1 mediates highly efficient Cre/loxP mediated recombination in the nervous system,
889 kidney, and somite-derived tissues. *Genesis* 44: 355-360, 2006.

890 64. **Verkhratsky A, Krishtal OA and Burnstock G**. Purinoceptors on neuroglia. *Mol Neurobiol* 39:
891 190-208, 2009.

892 65. **Yamada T and Strange K**. Intracellular and extracellular loops of LRRC8 are essential for volume-
893 regulated anion channel function. *J Gen Physiol* 150: 1003-1015, 2018. doi:
894 10.1085/jgp.201812016

895 66. **Liu HT, Tashmukhamedov BA, Inoue H, Okada Y and Sabirov RZ**. Roles of two types of anion
896 channels in glutamate release from mouse astrocytes under ischemic or osmotic stress. *Glia* 54:
897 343-357, 2006. doi: 10.1002/glia.20400

898 67. **Sabirov RZ, Merzlyak PG, Okada T, Islam MR, Uramoto H, Mori T, Makino Y, Matsuura H, Xie Y**
899 **and Okada Y**. The organic anion transporter SLCO2A1 constitutes the core component of the
900 Maxi-Cl channel. *EMBO J* 36: 3309-3324, 2017.

901 68. **Han YE, Kwon J, Won J, An H, Jang MW, Woo J, Lee JS, Park MG, Yoon BE, Lee SE, Hwang EM,**
902 **Jung JY, Park H, Oh SJ and Lee CJ**. Tweety-homolog (Ttyh) family encodes the pore-forming
903 subunits of the swelling-dependent volume-regulated anion channel (VRAC(swell)) in the brain.
904 *Exp Neurobiol* 28: 183-215, 2019. doi: 10.5607/en.2019.28.2.183

905 69. **Woo DH, Han KS, Shim JW, Yoon BE, Kim E, Bae JY, Oh SJ, Hwang EM, Marmorstein AD, Bae**
906 **YC, Park JY and Lee CJ**. TREK-1 and Best1 channels mediate fast and slow glutamate release in
907 astrocytes upon GPCR activation. *Cell* 151: 25-40, 2012.

908 70. **Oh SJ, Han KS, Park H, Woo DH, Kim HY, Traynelis SF and Lee CJ**. Protease activated receptor 1-
909 induced glutamate release in cultured astrocytes is mediated by Bestrophin-1 channel but not
910 by vesicular exocytosis. *Mol Brain* 5: 38, 2012.

911 71. **Ye ZC, Wyeth MS, Baltan-Tekkok S and Ransom BR**. Functional hemichannels in astrocytes: a
912 novel mechanism of glutamate release. *J Neurosci* 23: 3588-3596, 2003.

913 72. **Duan S, Anderson CM, Keung EC, Chen Y, Chen Y and Swanson RA**. P2X7 receptor-mediated
914 release of excitatory amino acids from astrocytes. *J Neurosci* 23: 1320-1328, 2003.

915 73. **Iglesias R, Dahl G, Qiu F, Spray DC and Scemes E**. Pannexin 1: the molecular substrate of
916 astrocyte "hemichannels". *J Neurosci* 29: 7092-7097, 2009.

917 74. **Syeda R, Qiu Z, Dubin AE, Murthy SE, Florendo MN, Mason DE, Mathur J, Cahalan SM, Peters**
918 **EC, Montal M and Patapoutian A**. LRRC8 proteins form volume-regulated anion channels that
919 sense ionic strength. *Cell* 164: 499-511, 2016. doi: 10.1016/j.cell.2015.12.031

920 75. **Concepcion AR, Wagner LE, Zhu J, Tao AY, Yang J, Khodadadi-Jamayran A, Wang YH, Liu M,**
921 **Rose RE, Jones DR, Coetzee WA, Yule DI and Feske S**. The volume-regulated anion channel
922 LRRC8C suppresses T cell function by regulating cyclic dinucleotide transport and STING-p53
923 signaling. *Nat Immunol* 23: 287-302, 2022. doi: 10.1038/s41590-021-01105-x

924 76. **Yu Q, Zhao Y, Maurer J, Arullampalam P, John N, Tranter JD, Abd El-Aziz TM, Lin M, Lerner DJ,**
925 **Halabi CM and Sah R**. Endothelial LRRC8C associates with LRRC8A and LRRC8B to regulate
926 vascular reactivity and blood pressure. *bioRxiv* https://doi.org/10.1101/2025.08.17.670763,
927 2025. doi: 10.1101/2025.08.17.670763

928 77. **Groulx N, Boudreault F, Orlov SN and Grygorczyk R**. Membrane reserves and hypotonic cell
929 swelling. *J Membr Biol* 214: 43-56, 2006.

930 78. **Li P, Hu M, Wang C, Feng X, Zhao Z, Yang Y, Sahoo N, Gu M, Yang Y, Xiao S, Sah R, Cover TL,**
931 **Chou J, Geha R, Benavides F, Hume RI and Xu H**. LRRC8 family proteins within lysosomes
932 regulate cellular osmoregulation and enhance cell survival to multiple physiological stresses.
933 *Proc Natl Acad Sci U S A* 117: 29155-29165, 2020.

934 79. **Kumar A, Zhao Y, Xie L, Chadda R, Tranter JD, Mikami RT, Abraham N, Hong J, Feng E,**
935 **Rawnsley DR, Liu H, Henry KM, Meyer G, Hu M, Xu H, Hinton A, Jr., Grueter CE, Abel ED, Norris**

936 **AW, Diwan A and Sah R**. Lysosomal LRRC8 complex impacts lysosomal pH, morphology, and
937 systemic glucose metabolism. *Sci Adv* 11: eadt6366, 2025. doi: 10.1126/sciadv.adt6366

938 80. **Ghosh A, Khandelwal N, Kumar A and Bera AK**. Leucine-rich repeat-containing 8B protein is
939 associated with the endoplasmic reticulum Ca(2+) leak in HEK293 cells. *J Cell Sci* 130: 3818-3828,
940 2017.

941 81. **Yanushkevich S, Zieminska A, Gonzalez J, Anazco F, Song R, Arias-Cavieres A, Granados ST, Zou**
942 **J, Rao Y and Concepcion AR**. Recent advances in the structure, function and regulation of the
943 volume-regulated anion channels and their role in immunity. *J Physiol* 2024. doi:
944 10.1113/JP285200

945 82. **Quinodoz M, Rutz S, Peter V, Garavelli L, Innes AM, Lehmann EF, Kellenberger S, Peng Z,**
946 **Barone A, Campos-Xavier B, Unger S, Rivolta C, Dutzler R and Superti-Furga A**. De novo variants
947 in LRRC8C resulting in constitutive channel activation cause a human multisystem disorder.
948 *EMBO J* 44: 413-436, 2025. doi: 10.1038/s44318-024-00322-y

949 83. **Ridder MC, Boor I, Lodder JC, Postma NL, Capdevila-Nortes X, Duarri A, Brussaard AB, Estevez**
950 **R, Scheper GC, Mansvelder HD and van der Knaap MS**. Megalencephalic leucoencephalopathy
951 with cysts: defect in chloride currents and cell volume regulation. *Brain* 134: 3342-3354, 2011.

952 84. **Capdevila-Nortes X, Lopez-Hernandez T, Apaja PM, Lopez de HM, Sirisi S, Callejo G, Arnedo T,**
953 **Nunes V, Lukacs GL, Gasull X and Estevez R**. Insights into MLC pathogenesis: GlialCAM is an
954 MLC1 chaperone required for proper activation of volume-regulated anion currents. *Hum Mol*
955 *Genet* 22: 4405-4416, 2013.

956 85. **Dubey M, Brouwers E, Hamilton EMC, Stiedl O, Bugiani M, Koch H, Kole MHP, Boschert U,**
957 **Wykes RC, Mansvelder HD, van der Knaap MS and Min R**. Seizures and disturbed brain
958 potassium dynamics in the leukodystrophy megalencephalic leukoencephalopathy with
959 subcortical cysts. *Ann Neurol* 83: 636-649, 2018.
960

# FIGURE LEGENDS

**Figure 1: LRRC8A-containing VRACs are the main conduit for swelling-activated release of cytosolic glutamate.**

**A**, Breeding strategy for brain-specific deletion of LRRC8A using *Nestin*$^{Cre}$ recombination. The four genotypes generated are: *Lrrc8a*$^{flox/+}$ (fl/+), *Lrrc8a*$^{flox/flox}$ (fl/fl), *Lrrc8a*$^{flox/+}$:*Nestin*$^{Cre/+}$ (HET), and *Lrrc8a*$^{flox/flox}$:*Nestin*$^{Cre/+}$ (KO). **B**, Representative live images of LRRC8A HET and KO astrocytes expressing the Cre reporter Ai9. TdTomato fluorescence was captured at 320× magnification. **C**, Representative full-length Western blot of LRRC8A immunoreactivity and matching β-actin signal in primary astrocyte cultures from the four genotypes shown in (A). **D**, Quantification of LRRC8A expression normalized to β-actin and presented relative to the average signal from fl/+ samples. Data are the mean values ± SD from five cultures per group. ****$p < 0.0001$, one-way ANOVA with Tukey's multiple comparisons test. **E**, VRAC activity in primary astrocytes assessed as swelling-activated release of D-[$^3$H]aspartate in response to a 30% reduction in medium osmolality (290 to 200 mOsm). Data are the mean values ± SD from 8-16 independent experiments in at least two different astrocyte cultures per genotype. *$p < 0.05$, ****$p < 0.0001$, HET (n=8) and KO (n=8) vs. controls (fl/+ and fl/fl, n=16), respectively. $^{\#\#}p < 0.01$, HET vs. KO. One-way ANOVA of maximal release values with Tukey's multiple comparisons test. **Inset**: Hypoosmotic response in LRRC8A KO astrocytes shown on an expanded scale. **F**, VRAC activity in primary astrocytes exposed to a 50% reduction in medium osmolality (from 290 to 150 mOsm). Data are the mean values ± SD from 8–11 independent experiments in at least two different astrocyte cultures per genotype. ****$p < 0.0001$, HET (n=9) and KO (n=8) vs. controls (fl/+ and fl/fl, n=11); $^{\#}p < 0.05$, HET vs. KO. One-way ANOVA with Tukey's multiple comparisons test. **Inset**: Hypoosmotic response in LRRC8A KO astrocytes shown on an expanded scale.

**Figure 2: Relative abundance of *Lrrc8a-e* transcripts in mouse brain and primary astrocyte cultures.**

**A**, Quantification of mRNA expression levels for *Lrrc8a-e* in mouse forebrain lysates using qRT-PCR. Expression levels were normalized to ribosomal *Rpl13a* within the same sample. Data are the mean values ± SD of seven mouse forebrains. **B**, RNA-seq analysis of *Lrrc8a-e* expression in seven mouse forebrain regions from five mice of both sexes (data downloaded from the Human Protein Atlas). **C**, Quantification of mRNA expression levels for *Lrrc8a-e* in primary astrocyte cultures measured with qRT-PCR and normalized to ribosomal *Rpl13a*. Data are the mean values ± SD of six independent cultures.

**Figure 3: Time Course of siRNA-mediated LRRC8A knockdown and its impact on swelling-activated glutamate release.**

**A1**, Representative Western blot of LRRC8A immunoreactivity and corresponding β-actin signal from protein lysates collected 24h, 48h, 72h, and 96h post siRNA transfection with either negative control siRNA (NC) or *Lrrc8a*-targeting siRNA (siA1). **A2**, Quantification of LRRC8A protein levels, normalized to β-actin and presented relative to the average signal from siNC samples. Data are the mean values ± SD from three independent transfections performed in three different astrocyte

1003 cultures. **B1**, Representative Western blot of LRRC8A immunoreactivity and matching β-actin
1004 signal from protein lysates collected 96h after treatment with siNC or one of three *Lrrc8a*-targeting
1005 siRNA constructs (siA1, siA3, or siA4). **B2**, Quantification of LRRC8A protein levels normalized
1006 to β-actin and presented relative to the average signal from siNC samples. Data are the mean
1007 values ± SD from four independent transfections performed in four different astrocyte cultures.
1008 ****$p < 0.0001$, **$p < 0.01$, one-way ANOVA with Tukey's multiple comparisons test. **C1**,
1009 Statistical comparison of the maximal D-[$^3$H]aspartate release values and area under the curve
1010 from C2. Data are the mean values ± SD in six independent transfections in two different astrocyte
1011 cultures per group. ****$p < 0.0001$, unpaired t-test. **C2**, Kinetics of VRAC-mediated D-
1012 [$^3$H]aspartate release from astrocyte cultures treated with siNC or siA1 and exposed to a 30%
1013 reduction in medium osmolality.

1014

1015 **Figure 4: Functional contribution of individual LRRC8A-E subunits to glutamate-**
1016 **permeable VRACs.**

1017 **A1**, Quantification of *Lrrc8a-e* mRNA expression levels in mouse astrocyte cultures treated with
1018 negative control siRNA (siNC). Expression levels were normalized to the housekeeping *Rpl13a*.
1019 Data are the mean values ± SD of four independently prepared cell cultures. **A2**, Schematic of a
1020 radiotracer assay of VRAC activity (created with BioRender.com, see Methods for additional
1021 details). **B-F**, Effects of gene-specific siRNA constructs on *Lrrc8a-e* mRNA expression levels 48
1022 h post-transfection and swelling-activated D-[$^3$H]aspartate release 96 h post transfection. ***B1-F1***,
1023 Relative *Lrrc8a-e* expression was normalized to *Rpl13a* and compared to siNC. Values are the
1024 means ± SD of 3-4 independent transfections in at least two different astrocyte cultures. ***$p <$
1025 $0.001$, **$p < 0.01$, *$p < 0.05$, one-population t-test with Bonferroni correction for multiple
1026 comparisons. ***B2-F2***, Integral D-[$^3$H]aspartate release values in cells exposed for 10 min to either
1027 isoosmotic (Basal) or hypoosmotic (Hypo) conditions (see Methods). With the exception of *F2*,
1028 data are the mean values ± SD of 6-9 independent transfections in two independently prepared
1029 cell cultures. For *Lrrc8e* knockdowns in *F2*, data are the mean values ± SD of three independent
1030 transfections in one astrocyte culture. ****$p < 0.0001$, *** $p < 0.001$, ** $p < 0.01$ vs. siNC, repeated
1031 measures two-way ANOVA with Tukey's multiple comparisons test (for clarity only the effect of
1032 siRNA under hypoosmotic conditions are shown).

1033

1034 **Figure 5: Validation of LRRC8C and LRRC8D protein loss following siRNA-mediated**
1035 **knockdown.**

1036 **A**, Representative full-length Western blot of LRRC8C immunoreactivity and corresponding β-
1037 actin signal from protein lysates prepared 96h post siRNA transfection with either siNC or siC1.
1038 **B**, Quantification of LRRC8C protein levels normalized to β-actin and presented relative to the
1039 average signal from siNC samples. Data are the mean values ± SD from four independent
1040 transfections performed in four different astrocyte cultures. ****$p < 0.0001$, unpaired t-test. **C**,
1041 Representative Western blot of LRRC8D immunoreactivity and corresponding β-actin signal from
1042 protein lysates prepared 96h post siRNA transfection with either siNC or siD4. **D**, Quantification
1043 of LRRC8D protein levels normalized to β-actin and presented relative to the average signal from
1044 siNC samples. Data are the mean values ± SD from four independent transfections performed in
1045 four different astrocyte cultures. ***$p < 0.001$, unpaired t-test.

1046 **Figure 6: LRRC8 knockdown modulates partner protein levels independently of mRNA**
1047 **changes**

1048 **A-D**, qRT-PCR analysis of all five *Lrrc8* transcripts in mouse astrocytes treated with the most
1049 effective siRNA constructs targeting *Lrrc8a-d* (siA1, siB4, siC1, and siD4). Relative *Lrrc8a-e*
1050 expression levels are normalized to *Rpl13a* within the same sample and compared to siNC,
1051 measured 48 h post-transfection. Data are the mean normalized values ± SD of 3-4 independent
1052 transfections. ***p < 0.001, **p < 0.01, *p < 0.05, one-population t-test with Bonferroni correction
1053 for multiple comparisons. **E**, Top: Quantification of LRRC8C and LRRC8D protein levels in control
1054 (*Lrrc8a*$^{fl/+}$) and LRRC8A KO astrocytes, normalized to β-actin and expressed relative to the mean
1055 signal in control samples. Data are the mean values ± SD from four independent cultures per
1056 group. ****p < 0.0001, ***p < 0.001; unpaired t-test. Bottom: Representative Western blot of
1057 LRRC8C or LRRC8D immunoreactivity and matching β-actin signal. **F**, Top: Quantification of
1058 LRRC8C and LRRC8D protein levels in astrocytes treated with siNC or siA1, normalized to β-
1059 actin and expressed relative to siNC. Data are the mean values ± SD from four independent
1060 cultures per group. ****p < 0.0001; unpaired t-test. Bottom: Representative Western blots of
1061 LRRC8C or LRRC8D and matching β-actin. **G**, Top: Quantification of LRRC8A and LRRC8D
1062 protein levels in astrocytes treated with siNC or siC1, normalized to β-actin and expressed relative
1063 to siNC. Data are the mean values ± SD from four independent cultures per group. **p < 0.01,
1064 unpaired t-test. Bottom: Representative Western blot of LRRC8A or LRRC8D immunoreactivity
1065 and matching β-actin signal. **H**, Top: Quantification of LRRC8A and LRRC8C protein levels in
1066 astrocytes treated with siNC or siD4, normalized to β-actin and expressed relative to siNC. Data
1067 are the mean values ± SD from four independent cultures per group. **p < 0.01; unpaired t-test.
1068 Bottom: Representative Western blot or LRRC8A or LRRC8C immunoreactivity and matching β-
1069 actin signal.

1070

1071 **Figure 7: Non-redundant roles of LRRC8C and LRRC8D subunits in glutamate-permeable**
1072 **VRACs.**

1073 **A**, Validation of siRNA efficacy in double knockdown experiments targeting *Lrrc8c* and *Lrrc8d*.
1074 Astrocytes were treated with siRNA targeting *Lrrc8c* (siC1), *Lrrc8d* (siD4), or their combination
1075 (siC1 + siD4). Efficacy of gene-specific knockdowns was verified by qRT-PCR. Data are the mean
1076 normalized expression values ± SD in three independently transfected cell cultures. **p < 0.01,
1077 *p < 0.05, one-population t-test with Bonferroni correction for multiple comparisons. **B**, Effect of
1078 siC1, siD4, or siC1+siD4 on VRAC-mediated D-[$^3$H]aspartate release from cultured astrocytes
1079 exposed to a 30% reduction in medium osmolality measured in a 12-well plate format. Data are
1080 the mean values ± SD from twelve independent transfections in three different astrocyte cultures.
1081 ****p < 0.0001 vs. siNC, repeated measures two-way ANOVA with Tukey's multiple comparisons
1082 test (only the effects of siRNAs under hypoosmotic conditions are shown). **C**, Kinetics of VRAC-
1083 mediated D-[$^3$H]aspartate release from astrocyte cultures treated with siNC, siC1, siD4, or
1084 siC1+siD4 and exposed to a 30% reduction in medium osmolality. Data are the mean values ±
1085 SD in 6-11 independent transfections performed in three different astrocyte cultures. **Inset**:
1086 Statistical comparison of the maximal D-[$^3$H]aspartate release values (top) and area under the
1087 curve (bottom) in the same experiments. ****p < 0.0001, ***p < 0.001, **p < 0.01, one-way ANOVA
1088 with Tukey's multiple comparisons test. **D**, Kinetics of VRAC-mediated D-[$^3$H]aspartate release
1089 from astrocytes treated with siNC, siC1, siD4, or siC1+siD4 and exposed to a 50% reduction in
1090 medium osmolality. Data are the mean values ± SD in 5-6 independent transfections performed

1091 in two different astrocyte cultures. **Inset**: Statistical comparison of the maximal D-[$^3$H]aspartate
1092 release values (top) and area under the curve (bottom) in the same experiments. ****p < 0.0001,
1093 **p < 0.01, one-way ANOVA with Tukey's multiple comparisons test.

1094

1095 **Figure 8: Functional contribution of LRRC8B to LRRC8C- and LRRC8D-containing**
1096 **VRACs.**

1097 **A**, Validation of siRNA efficacy in double knockdown experiments targeting *Lrrc8b* and *Lrrc8c*.
1098 Astrocytes were treated with siRNA targeting *Lrrc8b* (siB4), *Lrrc8c* (siC1), or their combination
1099 (siB4+siC1). Efficacy of gene-specific knockdowns was verified by qRT-PCR. Data are the mean
1100 normalized expression values ± SD in three independently transfected cell cultures. **p < 0.01,
1101 *p < 0.05; one-population t-test with Bonferroni correction for multiple comparisons. **B**, Effects of
1102 siNC, siB4, siC1, siB4+siC1 on VRAC-mediated D-[$^3$H]aspartate release from cultured astrocyte
1103 exposed to a 30% reduction in medium osmolality, measured in a 12-well plate format. Data are
1104 the mean values ± SD from six independent transfections in two different astrocyte cultures. ****p
1105 < 0.0001, repeated measures two-way ANOVA with Tukey's multiple comparisons test (only the
1106 effects of siRNAs under hypoosmotic conditions are shown). **C**, Top: Quantification of LRRC8C
1107 protein levels in astrocytes treated with siNC or siB4, normalized to β-actin and expressed relative
1108 to siNC. Data are the mean values ± SD from four independent cultures per group. *p < 0.05;
1109 unpaired t-test. Bottom: Representative Western blot of LRRC8C and matching β-actin. **D**, qRT-
1110 PCR validation of double siRNA knockdown experiments targeting *Lrrc8b* (siB4) and *Lrrc8d*
1111 (siD4). Astrocytes were treated with siB4, siD4, or their combination (siB4+siD4). Data are the
1112 mean normalized expression values ± SD in three to four independently transfected cell cultures.
1113 ***p < 0.001, one-population t-test with Bonferroni correction for multiple comparisons. **E**, Effects
1114 of siNC, siB4, siD4, siB4+siD4 on VRAC-mediated D-[$^3$H]aspartate release from cultured
1115 astrocyte exposed to a 30% reduction in medium osmolality measured in a 12-well plate format.
1116 Data are the mean values ± SD from six independent transfections in two different astrocyte
1117 cultures. ****p < 0.0001, ***p < 0.001; repeated measures two-way ANOVA with Tukey's multiple
1118 comparisons test (only the effects of siRNAs under hypoosmotic conditions are shown). **F**, Top:
1119 Quantification of LRRC8D protein levels in astrocytes treated with siNC or siB4, normalized to β-
1120 actin and expressed relative to siNC. Data are the mean values ± SD from four independent
1121 cultures per group, unpaired t-test. Bottom: Representative Western blot LRRC8D and matching
1122 β-actin.

1123

1124 **Figure 9: Proposed subunit composition of glutamate-permeable VRACs in astrocytes.**

1125 **A** and **B**, Theoretical predictions of the effects on siRNA knockdowns on VRAC activity based on
1126 two models of VRAC composition. In *Model I*, VRACs are assembled from LRRC8A, LRRC8C,
1127 and LRRC8D subunits, with LRRC8C and LRRC8D functioning as mutually redundant
1128 components. In *Model II*, two independent VRAC populations are formed by either
1129 LRRC8A+LRRC8C or LRRC8A+LRRC8D. In this case, LRRC8C and LRRC8D subunits are not
1130 functionally redundant. **C**, *Experimental outcomes* showing the effects of LRRC8C (siC) and/or
1131 LRRC8D (siD) knockdown on VRAC-mediated D-[$^3$H]aspartate release in mouse astrocytes
1132 subjected to moderate (30% reduction in osmolarity; light bars) or severe (50% reduction in
1133 osmolarity; dark bars) hypotonic stress (data from Fig. 7C and 7D). These results are consistent
1134 with the Model II in which two distinct VRAC populations mediate glutamate permeability.

1135 LRRC8A+LRRC8D-containing VRACs provide a smaller contribution to swelling-activated
1136 glutamate release, and their activity is dependent on the degree of cellular swelling. **$p < 0.01$,
1137 *$p < 0.05$; two-way ANOVA with Tukey's multiple comparisons test.

1138

1139

1140 # TABLES

1141 **Table 1.** qRT-PCR primers used for gene expression analysis.

| Primer target | Primer ID | Source | GeneGlobe ID |
|---|---|---|---|
| *Rpl13a* (housekeeping) | Mm_Rpl13a_1_SG | Qiagen | QT00267197 |
| *Rps20* (housekeeping) | Mm_Rps20_1_SG | Qiagen | QT00251433 |
| *Gapdh* (housekeeping) | Mm_Gapdh_3_SG | Qiagen | QT01658692 |
| *Lrrc8a* | Mm_Lrrc8a_2_SG | Qiagen | QT01167502 |
| *Lrrc8b* | Mm_Lrrc8b_1_SG | Qiagen | QT01541666 |
| *Lrrc8c* | Mm_Lrrc8c_1_SG | Qiagen | QT01042881 |
| *Lrrc8d* | Mm_Lrrc8d_1_SG | Qiagen | QT02255085 |
| *Lrrc8e* | Mm_Lrrc8e_1_SG | Qiagen | QT01046269 |

1142

1143 **Table 2.** Primary and secondary antibodies used for western blot analysis.

| Protein target | Species/type | Source | Catalog # | RRID | Dilution |
|---|---|---|---|---|---|
| β-actin, HRP-conjugated | Mouse, monoclonal | Millipore-Sigma | A3854 | AB_262011 | 1:50,000 |
| LRRC8A | Mouse monoclonal | Santa Cruz Biotech. | sc-517113 | AB_2928142 | 1:1,000 |
| LRRC8C | rabbit polyclonal | Proteintech | 21601-1-AP | | 1:2,000 |
| LRRC8D | rabbit polyclonal | Proteintech | 11537-1-AP | AB_2137767 | 1:2,000 |
| anti-mouse IgG, HRP-conjugated | sheep | GE Healthcare | NA931 | | 1:10,000 |
| anti-rabbit IgG, HRP-conjugated | donkey | GE Healthcare | NA934 | | 1:10,000 |

1144

1145

1146 **Table 3.** siRNA constructs used in RNAi experiments.

| siRNA target | siRNA name | Abbr. | Source | GeneGlobe ID | Sequence |
|---|---|---|---|---|---|
| Negative Control | AllStars Negative Control siRNA | siNC | Qiagen | SI03650318 | Proprietary |
| *Lrrc8a* | Mm_Lrrc8_1 | siA1 | Qiagen | SI01296127 | CAGCCTCAAGAAGATGGTTAA |
| | Mm_Lrrc8_3 | siA3 | Qiagen | SI01296141 | CAGAGTCATCTCAGGGTTAAA |
| | Mm_Lrrc8_4 | siA4 | Qiagen | SI01296148 | AATGATGGTTTGGGTATTAAA |
| *Lrrc8b* | Mm_LOC433926_1 | siB1 | Qiagen | SI01235311 | AAGAAGATGGTCAATCTGAAA |
| | Mm_LOC433926_3 “ | siB3 | Qiagen | SI01235325 | ATCCTGTTTGTCCTTATTATA |
| | Mm_LOC433926_4 | siB4 | Qiagen | SI01235332 | TAGGAGGATGAACTTTCCTAA |
| *Lrrc8c* | Mm_E430036I04Rik_1 | siC1 | Qiagen | SI00988799 | ATCGGAGTTCTGCAAAGTTTA |
| | Mm_E430036I04Rik_2 | siC2 | Qiagen | SI00988806 | GAGAAGTAACATATACATATA |
| | Mm_E430036I04Rik_4 | siC4 | Qiagen | SI00988820 | CACCTTATACTGGCTGTTCTA |
| *Lrrc8d* | LRRC5_1 | siD1 | Qiagen | SI01296043 | TTGCAAGTTATTACAAGATAA |
| | LRRC5_2 | siD2 | Qiagen | SI01296050 | CAGCATGACAATCCTGGACAA |
| | LRRC5_4 | siD4 | Qiagen | SI01296064 | AAGCCCTGTTTGAGAAAGTAA |
| *Lrrc8e* | Mm_1810049O03Rik_1 | siE1 | Qiagen | SI00806043 | CACATTTAGCTATGTAATAAA |
| | Mm_1810049O03Rik_2 | siE2 | Qiagen | SI00806050 | CTGAAGGTGATCTGTGTTAAA |
| | Mm_1810049O03Rik_4 | siE4 | Qiagen | SI00806064 | CCCAACAAGGATCAGCATATA |

1147

1148

Figure 1 • M.L. Chandler *et al.*

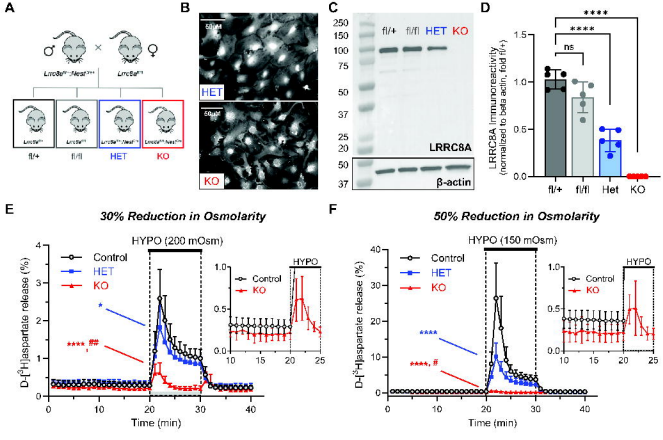

Figure 2 • M.L. Chandler *et al.*

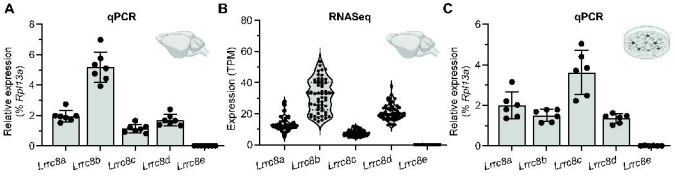

Figure 3 • M.L. Chandler *et al.*

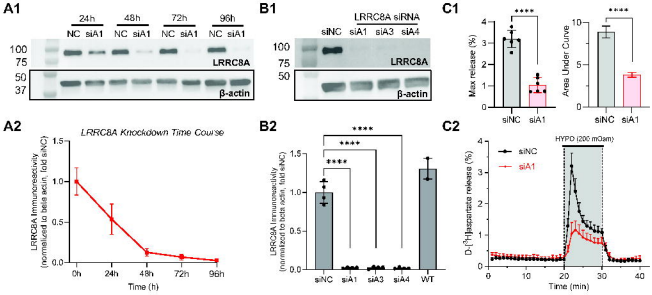

Figure 4 • M.L. Chandler *et al.*

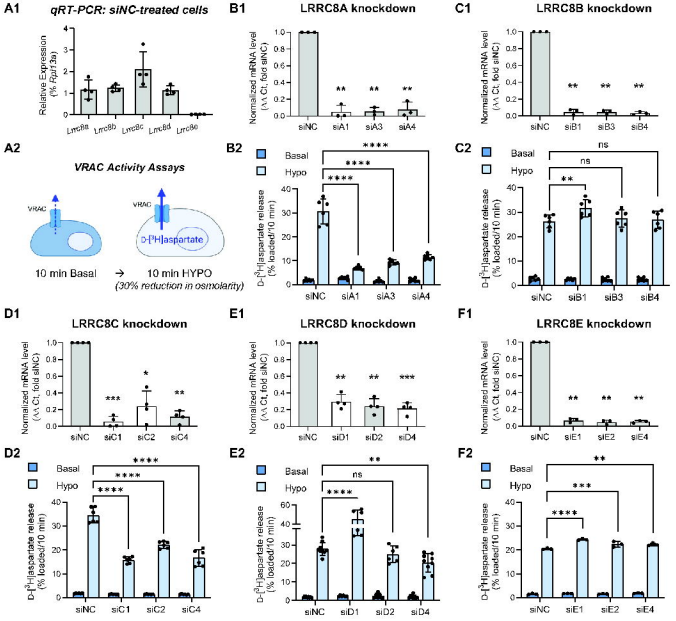

Figure 5 • M.L. Chandler *et al.*

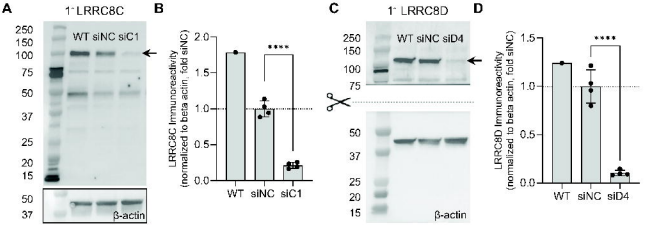

Figure 6 • M.L. Chandler *et al.*

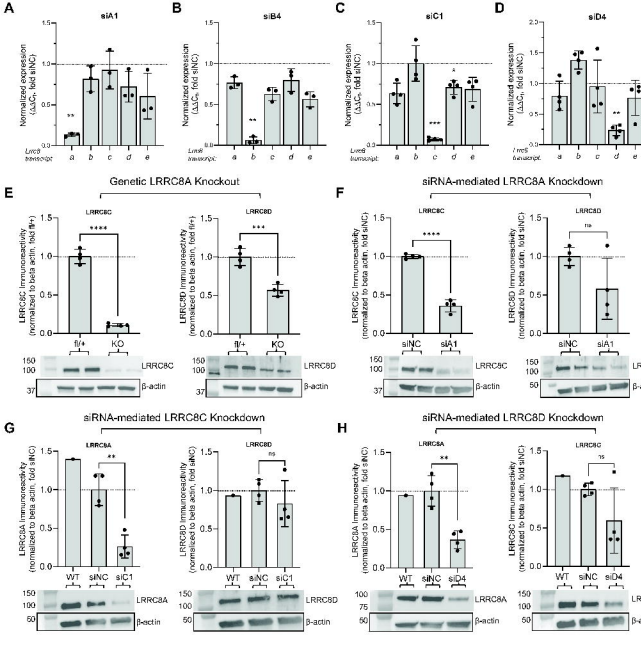

Figure 7 • M.L. Chandler et al.

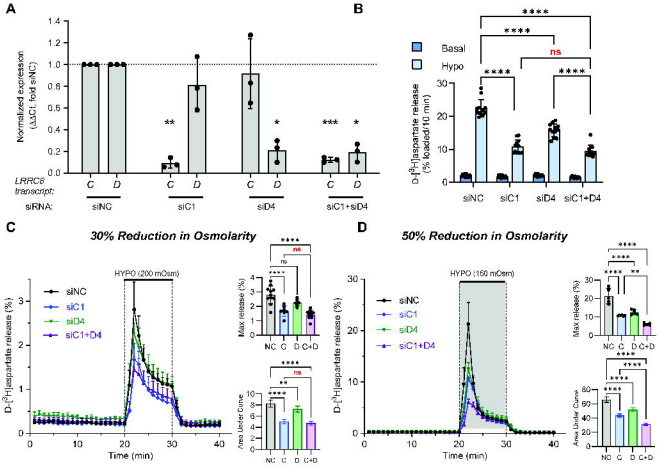

Figure 8 • M.L. Chandler et al.

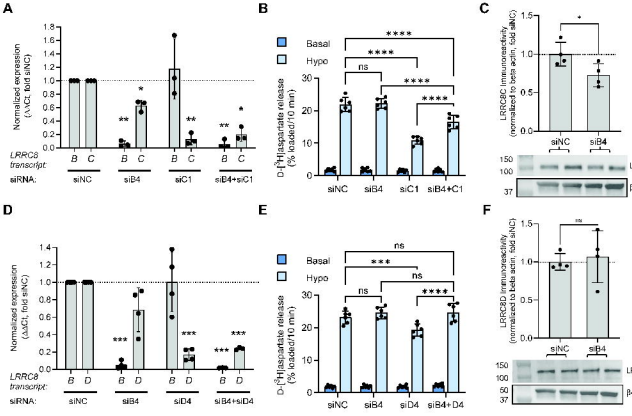
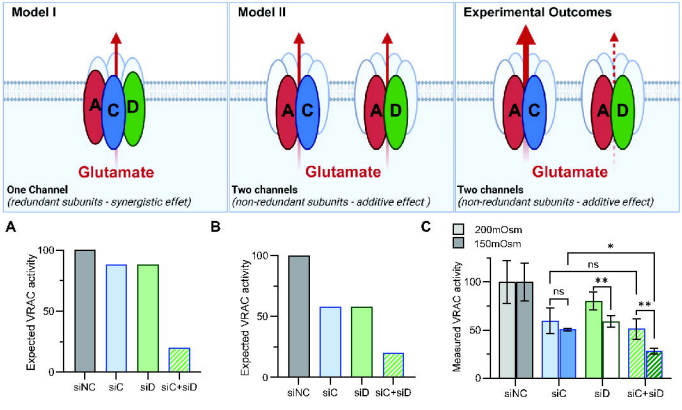
Figure 9 • M.L. Chandler et al.